




Article

The Numerical Investigations of Heat Transfer and Bubble Behaviors of R22 in Subcooled Flow Boiling in Casing Tubes

Xiaodie Hu ^{1,2} , Jinfeng Wang ^{1,2,3,4,*} , Jing Xie ^{1,2,3,4,*} , Bingjun Wang ^{1,2} and Fei Wang ¹

¹ College of Food Science and Technology, Shanghai Ocean University, Shanghai 201306, China; 2035203@st.shou.edu.cn (X.H.); m200300788@st.shou.edu.cn (B.W.); 1932124@st.shou.edu.cn (F.W.)

² Shanghai Professional Technology Service Platform on Cold Chain Equipment Performance and Energy, Saving Evaluation, Shanghai 201306, China

³ National Experimental Teaching Demonstration Center for Food Science and Engineering, Shanghai Ocean University, Shanghai 201306, China

⁴ Quality Supervision, Inspection and Testing Center for Cold Storage and Refrigeration Equipment, Ministry of Agriculture, Shanghai 201306, China

* Correspondence: jfwang@shou.edu.cn (J.W.); jxie@shou.edu.cn (J.X.); Tel.: +86-15692165513 (J.X.)

Abstract: Amidst the background of “double carbon”, energy saving and emission reduction is a popular direction in the current refrigeration industry. Therefore, the research on the boiling heat transfer of gas–liquid two-phase flow is helpful to strengthen the heat transfer and design a more efficient heat exchanger. In this paper, a research method combining numerical simulation and experimental verification is adopted. Firstly, an experimental platform used for the subcooled flow boiling of refrigerant in casing tubes is introduced and experiments are carried out to obtain experimental data, which provides a theoretical basis for the development of numerical simulation and verifies the feasibility of numerical simulation. A numerical model of subcooled flow boiling in R22 was established and the grid independence test was carried out. Based on the simulation results, three factors affecting the boiling heat transfer of R22 are analyzed: First, the boiling heat transfer coefficient of R22 increases with the increase of the mass flow rate of R22, but the increase decreases when the mass flow rate increases from 0.018 kg/s to 0.020 kg/s. Second, the boiling heat transfer coefficient of R22 increases significantly with the increase of hot water flow rate. Third, the influence of R22 subcooling on boiling heat transfer is more complex. When the subcooling is 5 °C and 1 °C, heat transfer can be enhanced; high subcooling at 5 °C can enhance convective heat transfer and low subcooling at 1 °C can accelerate the arrival of saturated boiling. In this paper, three kinds of bubble behaviors affecting heat transfer in supercooled flow boiling, including sliding, polymerization, and bounce are also studied, which provides a basis for further research on heat transfer mechanism of supercooled flow boiling.

Keywords: numerical simulation; gas–liquid flow; subcooled flow boiling; volume of fluid



Citation: Hu, X.; Wang, J.; Xie, J.; Wang, B.; Wang, F. The Numerical Investigations of Heat Transfer and Bubble Behaviors of R22 in Subcooled Flow Boiling in Casing Tubes. *Processes* **2023**, *11*, 2357. <https://doi.org/10.3390/pr11082357>

Academic Editors: Olga Soloveva and Sergei Solovev

Received: 6 July 2023

Revised: 29 July 2023

Accepted: 1 August 2023

Published: 5 August 2023



Copyright: © 2023 by the authors. Licensee MDPI, Basel, Switzerland. This article is an open access article distributed under the terms and conditions of the Creative Commons Attribution (CC BY) license (<https://creativecommons.org/licenses/by/4.0/>).

1. Introduction

Multiphase flow physics, a developing field of study known as physics, which is crucial to the advancement of technology and the social economy, was founded on the principles of fluid mechanics, heat and mass transport, physical chemistry, combustion science, and other fields. One of the key subfields of multiphase flow physics is two-phase flow, particularly gas–liquid biphasic flow, which finds widespread application in the energy, nuclear, petrochemical, low-temperature refrigeration, cooling of microelectronic devices, environmental protection, and aerospace industries [1].

Subcooling boiling occurs when the unsaturated liquid flowing into the tube is heated by the tube wall, and the liquid near the wall reaches a temperature above saturation and begins to bubble even though the main body of the liquid has not yet reached saturation. The fluid enters the saturated nucleation boiling zone, which encompasses the bubbly flow

and the block flow, if heating is allowed to continue until the major stream reaches the saturation temperature [2]. On the heated walls, the bubbles begin to form and expand until they separate from the walls. However, the bubbles may fall into the main stream because of the predominant flow's lower temperature. A portion of the fluid changes phases as a result of flow subcooling and boiling, and the resulting bubbles must absorb the latent heat of vaporization while disrupting the connected layer of fluid, enhancing the pipeline's ability to transport heat [3]. The most significant influencing factors in in-tube subcooled boils are temperature, mass flow, and pressure.

The processes of single-phase fluid heat transfer and gas–liquid two-phase heat transfer are both involved in subcooled boiling heat transfer, which is a more complex process due to the interaction of these two heat transfer modes [4]. Figure 1 shows the boiling partition of the subcooled flow. The working fluid in the supercooled state is continuously heated after entering the heating channel with a constant heat flux density. The wall temperature T_w and the liquid temperature T_l increase continuously. The heat transfer mode in region AB is single-phase flow heat transfer. Point B is the first point where the bubble begins to produce stably but does not break away in the heating channel, which is called the Onset of Nucleate Boiling (ONB). Onset of Nucleate Boiling (ONB) refers to the transition of heat transfer mode from the single-phase liquid convection to a combination of convection and nucleate boiling. It is identified by the formation of vapor bubbles in a pool of liquid or during a flow. Because the heat transfer capacity of nucleate boiling is higher than that of single-phase flow heat transfer, the wall temperature will decrease to a certain extent when subcooled boiling occurs. The region between point B and point C is the partially developed boiling (PDB) region. In this region, the temperature of the inner wall rises gradually until the bubble begins to separate from the heating wall, and the wall temperature will gradually stabilize. In the partially developed boiling region, the heat transfer between the heating wall and the fluid includes single-phase flow heat transfer and nucleate boiling heat transfer, but the proportion of single-phase flow heat transfer decreases with the increase of bubbles. The region between point C and point D is the fully developed boiling (FDB) region. In the fully developed boiling region, the temperature of the mainstream liquid will continue to rise until it reaches saturation temperature. In this region, nucleate boiling is the main heat transfer mode, and single-phase flow heat transfer almost no longer exists [5].

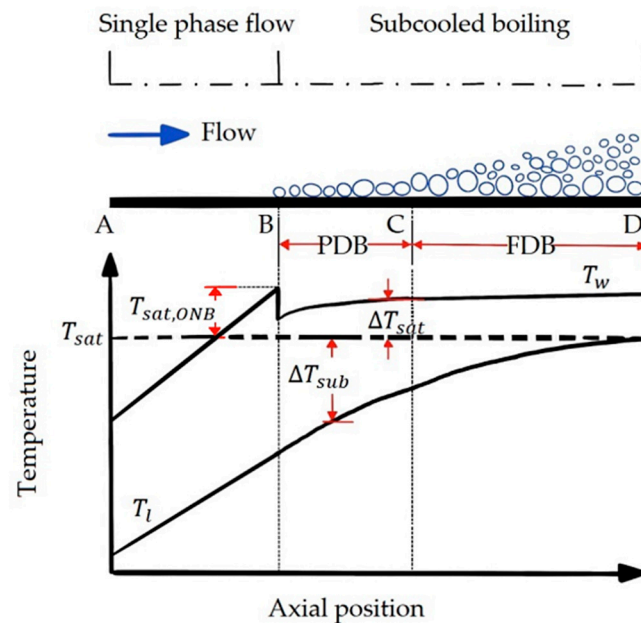


Figure 1. The boiling partition of the subcooled flow.

Experimental evaluations of several 95 CHF tables, models, and formulas for the boiling critical heat flow density of subcooled flow were conducted by H.X. Zhang et al. [6]. The vacuole share and bubble size of the gas–water two-phase under the boiling condition of the subcooled flow in the heated riser tube by CFX were numerically simulated by Wang Xiaojun et al. [7] and experimentally verified. The boiling heat transfer coefficients of R32, R134a [8] pure, R32 mixed with R134a, and R32 mixed with R125 were calculated by Shin et al. [9] and compared to the predictions of the Gungor and Winterton correlation equation [10,11]. Experimental research on the flow boiling of R134a in a copper tube with a diameter of 1.1 mm was carried out by Shiferaw et al.

R134a flow boiling tests were carried out by Saisorn et al. [12] in a spherical stainless steel tube with an inner diameter of 1.75 mm. Wang Smin et al. [13] used CFX 3.1 software to numerically simulate the subcooled boiling heat exchange of liquid nitrogen in a vertical circular tube, compared the results to experimental data, and improved the numerical simulation model of subcooled flow boiling based on the boiling heat exchange mechanism. They also established a subcooled boiling calculation model which is applicable to liquid ammonia.

The flow boiling heat transfer properties of R123 and R134a were assessed by In and Jeong [14] in a horizontal circular tube with an inner diameter of 0.19 mm. The findings of the experiment demonstrated that early boiling of R123 in the nucleated state was prevented and that as the dryness grew, the superheat of the tube wall also increased. This resulted in a rise in the intensity of the liquid film's evaporation, which enhanced the heat transfer coefficient.

The interface capture approach originated from the necessity to tackle several complicated multiphase flow issues and the limitations of single-phase flow simulation in the development of CFD. Each side of the contact is a single-phase flow problem since there is only one fluid present on each side. The two-phase flow issues can be resolved by coupling the flow at the relationship of the two fluids using the interface capture method, as long as the single-phase flow equations are specified for each side of the fluid. Different interface capture techniques are appropriate for diverse application contexts since they each have their own benefits and drawbacks.

Many different interface capture methods have been put forth by academics in the development of multiphase flow computational techniques, including the Particles in Fluid Method, which was first proposed by Harlow and Welch [15], the Level Set Method [16], and the Volume of Fraction (VOF) [17,18] method. According to the flow phase labeling approach, labeling points are added to various flow phases to help differentiate them from one another. The common edge of two grids is the interface between the two fluid phases when one grid has marker points and its neighboring grid does not. The fluid phase labeling approach can be used to simulate both large-scale and minute multiphase flows, such as droplet fragmentation [19]. However, the numerical simulation computation of actual engineering does not use the flow phase labeling method.

In order to solve incompressible two-phase flow issues, Dai et al. [20] introduced a level set method, where the intricate interface between the two flow phases is represented as a smooth curve with a level set function value of 0. The level set approach redefines the interface as a collection of virtual functions taking a certain value, for which a variety of ready-made numerical techniques are provided, converting a description of an interface change into a description of a change in a virtual function.

The VOF method introduces a novel fundamental concept for the building of phase interfaces and establishes new numerical simulation techniques for kinematic phase interfaces. The VOF method uses less hardware and takes up less computer storage space when compared to other approaches, especially when working with 3D issues. The VOF method is superior to other phase interface tracking methods when dealing with the fusion and fragmentation of complex phase interfaces and 3D phase interfaces due to its simple calculation and clear phase interface, which can represent the structure and changes of

complex phase interfaces. As a result, it can be used for many simulations of real-world engineering [21].

The majority of research on multiphase flow systems is constrained by particular circumstances due to their complexity, and the majority of the conclusions are empirical and semi-empirical correlations. Scholars have given CFD modeling a lot of attention since it can theoretically be investigated using multiphase flow and can eliminate a huge number of experiments. Due to its simplicity in calculation, the Euler–Euler model, also known as the two-fluid model, is frequently used to simulate gas–liquid two-phase flow [22]. Fluid includes the Mixture, Euler, and Volume of Fluid (VOF) models as its three Euler–Euler models. The three models can each be used for various Table 1 scenarios.

Table 1. The advantages and applicable scenarios of the three models in FLUENT.

Model	Merit	Applicable Scene
Mixture simulation	different velocities of each phase can be simulated	particle flow with low load and bubble flow with volume fraction
Eulerian model	precision is high	granular fluid, fluidized bed
VOF model	it takes up less memory, simple and effective	bubble-containing liquid, fluid after dam break

The most intricate multiphase flow model in FLUENT is the Eulerian model. The model becomes more difficult since each phase must solve a system of equations made up of n momentum equations and a continuum equation, where the pressure terms and intersection exchange coefficients are connected. There are different coupling modes for flow–solid granular flows and flow–flow non-granular flows, depending on the enclosed phases. Molecular dynamics [23] can be used to examine the flow characteristics of granular flows. The exchange of momentum among the various phases has an impact on the mixture’s class as well. The Eulerian model can be used to solve issues with fluidity beds, bubble columns, upwelling, and particle suspension.

The VOF model is an interface tracking technique based on an Eulerian grid that can be used to simulate the interaction of two fluids that are incompatible with one another. By resolving a series of momentum equations and monitoring the volume fraction of each fluid in the computational domain, the VOF model is applied to represent two fluids. The model can be used to track issues at the gas–liquid interface that are steady-state or transient, such as jet fragmentation, bubble motion in the liquid, and liquid motion following a dam break. It benefits from low memory usage and simple, quick calculations.

The two-phase flow for the VOF model has been investigated and simulated by numerous academics in China and worldwide. Wang et al. used the MHRIC method to calculate the face flow volume to describe the interface location of the two-phase flow, the finite volume method to spatially discretize the incompressible viscous RANS equation, and the VOF control equation in order to speed up the use of numerical simulations to solve the two-phase flow junction capture problem. By just providing the beginning values of pressure and velocity as well as the boundary conditions of velocity, the pressure solution time can be drastically decreased. A two-dimensional VOF model and a three-dimensional interface tracking model were compared by Yang et al. [24] to examine the rising motion and rising velocity of bubbles of various sizes as well as the impact of physical characteristics like density. L.S. Fan et al. [25,26]’s simulations of the behavior of individual bubbles in a high-pressure fluid revealed how the bubbles formed, rose, and collapsed along with their forms at each stage. W. Dijkhuizen et al. [27] studied the behavior of bubbles under fluids with high density, viscosity, and surface tension, focusing on the bubble aggregation phenomenon. They used the VOF approach for interfacial trapping among simulations.

In this paper, the subcooling boiling of R22 in casing tubes is investigated using a mix of numerical simulation and experimental verification. The novelty of the paper is that it combines the volume of fraction (VOF) model, level set method, Lee phase change model, and SST k - ω turbulent model for simulation experiments and observes the evolution of bubbles. The evolution of bubbles can not be observed in the actual experiment. In this

paper, the behavior and force characteristics of three types of bubbles (sliding, coalescing, and bouncing) in subcooled boiling are also analyzed in detail. The investigation of the bubble sliding dynamics is of great importance to effectively control the sliding process and enhance heat transfer. The condensation heat transfer of bubbles in subcooled boiling directly affects the direction of bubble evolution. The departure diameter increased with increased heat flux because the bubble absorbed heat from the heating wall during the sliding process. Therefore, the condensation heat transfer is obtained by experimental methods to predict the bubble evolution in subcooled boiling. By analyzing the bubble behavior of subcooled boiling in R22 tubes, the heat transfer process can be better revealed and the heat transfer efficiency can be improved. In this paper, the design of experimental methods and the establishment of numerical models can provide a method for the study of subcooled flow and also provide a theoretical basis for the design of high-efficiency heat exchangers. More importantly, the method of combining simulation research and experimental verification is adopted, which not only ensures the accuracy and reliability of the experimental results, but also expresses the experiment intuitively.

2. Materials and Methods

Relevant experimental experiments must be carried out in order to investigate the subcooling flow and boiling heat transfer properties of the refrigerant R22 and confirm the viability of the constructed CFD model. The amount of condensation heat exchange that the bubbles in subcooled boiling experience has a direct impact on the direction in which they evolve. Therefore, the condensation heat exchange is measured experimentally in order to make this prediction.

2.1. Introduction of the Experimental System

2.1.1. Experimental System

The system design for this experiment is illustrated in Figures 2 and 3. Both a water circulation system and a refrigerant circulation system are included in this testing bench. The preheat treatment cycle, test section water cycle, and chilled water cycle are all parts of the water circulation system. The same glycol cryogenic tank is used for the preheating cycle, condensation cycle, and subcooling cycle, which can lower the cost of experimental equipment and minimize the size of the test bench. Additionally, the test section can also be used to observe the state of refrigerant import and export with sight glasses S3 and S4. The plate heat exchanger HE2 and diaphragm metering pump inlet are connected with sight glasses S1 and S2, which are used to observe the refrigerant entering the plate heat exchanger HE2 and diaphragm metering pump before the state.

The glycol cryogenic water tank, Y-filter, and cryogenic circulation pump are all parts of the chilled water cycle, which consists of the pre-cooling treatment cycle, condensation treatment cycle, and subcooling treatment cycle. It also includes the plate heat exchanger, electromagnetic flow meter GW3, heat exchanger HE1, and condensation heat exchanger HE3. The plate heat exchanger HE2, the condensing heat exchanger HE3, and the heat exchanger HE1 are opened when the subcooled boiling experiment is conducted. The low-temperature circulating water pump removes chilled water from the glycol low-temperature tank after it has been first filtered through the Y-filter to remove impurities. This reduces the subcooling of the refrigerant liquid through the plate heat exchanger HE2, which then condenses the refrigerant vapor in the condensing heat exchanger HE3. The glycol cryogenic tank's chilled water exits and travels through the heat exchanger HE1 for heat exchange with the test section's heated water during the condensation experiment, while the plate heat exchanger HE2 and the condensing heat exchanger HE3 are shut off.

The glycol water solution in the glycol cryogenic tank uses distilled water and glycol for proportioning, which may remove the error caused by water impurities in the results of experiments and also stop the water from condensing in cold to effect heat exchange. In order to help with the requirement to modify the temperature in the experiment, the water

tank also has an adjustable power electric heater that may be used as a precision heater to control and fine-tune the water temperature.



Figure 2. Single tube boiling test systems.

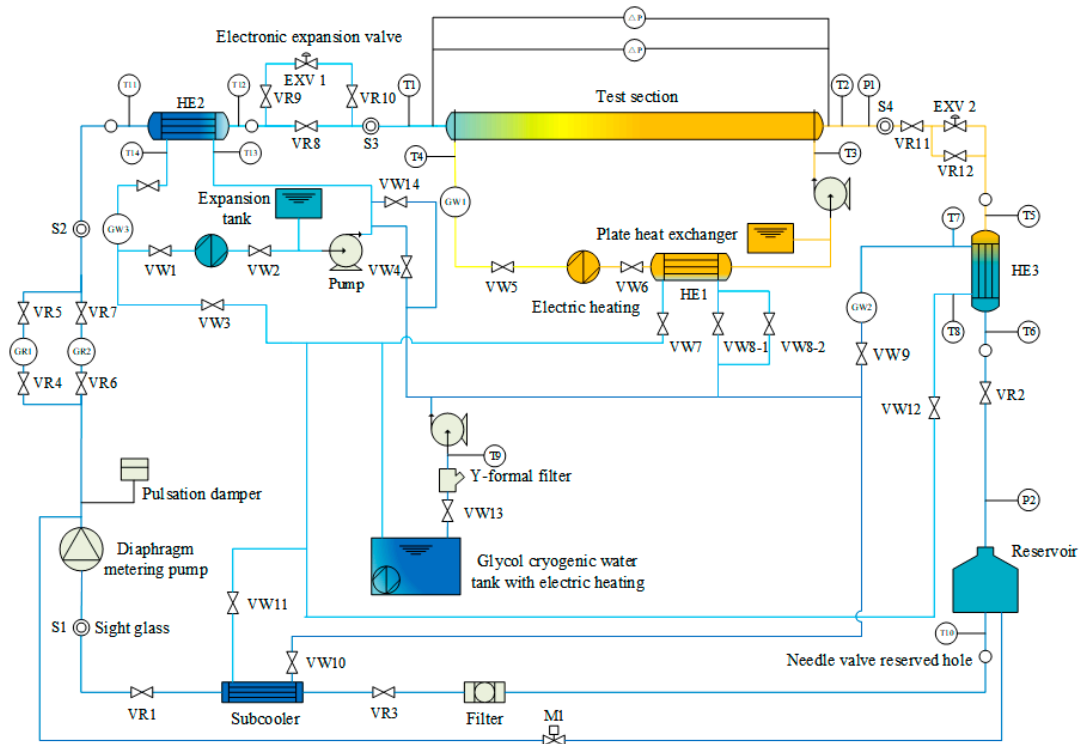


Figure 3. Experimental system diagram.

Instead of a conventional compressor, this laboratory bench employs a hydraulic diaphragm pump, which has the advantages of being more resource-efficient and quieter. It

is also more suitable for the inside climate of a laboratory and has the potential to operate in an oil-free state.

The models of important parts of the laboratory table are shown in Table 2.

Table 2. Types of important components of test bench.

Name	Type	The Name of the Manufacturer	The City of the Manufacturer	Country of Origin of Equipment
light horizontal multistage centrifugal pump	CHL2-40LSWSC	South Pump Industry Company	Wuxi	China
horizontal circulating water pump	MHI204-380V	Shanghai Bella Machinery Equipment Company	Shanghai	China
diaphragm metering pump	YSJ90LB4-1HS	Shanghai Xukai Electrical Equipment Company	Shanghai	China
ripple damper	HLMZ-MS0.6/5.0	Guangzhou Tuoyue Environmental Protection Equipment Company	Guangzhou	China
heat exchanger	CB30-22H-F	Alfa Laval Company	Shanghai	China
plate heat exchanger	ACH-30EQ-50HF	Shanghai Suyun Trading Company	Shanghai	China
condensing heat exchanger	AC-30EQ-44HF	Shanghai Suyun Trading Company	Shanghai	China
drier filter	EMERSON EK-164S	EMERSON Company	Missouri	USA
subcooler	SS-0075GT-U	Hangzhou HZSS Company	Hangzhou	China
frequency converter	6SE6440-2UD15-5AA1	Changzhou Hechang Mechanical & Electrical Company	Changzhou	China
pressure regulator	PAC35C-B160-90A-11	SHIMADEN Technology Company	Beijing	China
electric heating	PAC35C-90A	SHIMADEN Technology Company	Beijing	China
electronic expansion valve	ETS 6	Danfoss Company	Shanghai	China

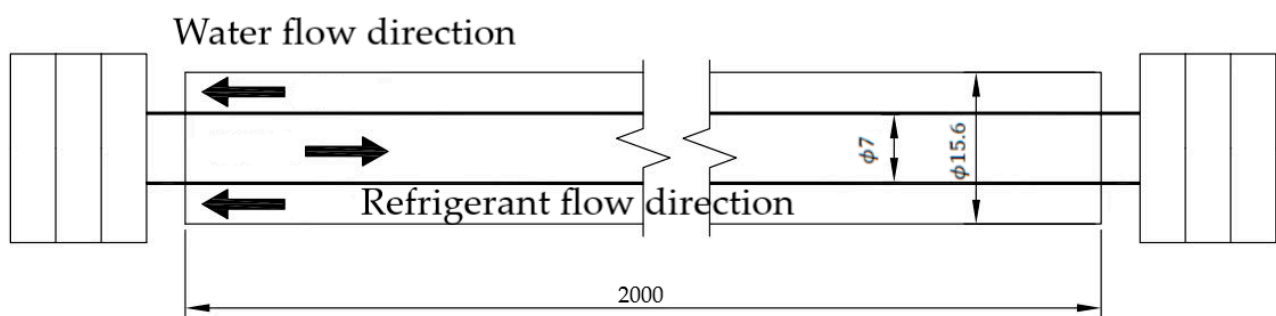
The acquisition of parameters in refrigerant single-tube boiling experiments, such as temperature, pressure, and flow rate, is essential for the analysis of experimental findings and provides a foundation for further simulations. Temperature, pressure, and flow signals are gathered by the test bench using differential pressure sensors, PT100 platinum resistors, electromagnetic flow meters, and mass flow meters. The pressure drop in the test portion is measured using the differential pressure sensor. In order to measure temperature and obtain more precise temperature data, a four-wire Pt100 platinum resistor with good stability, good pressure resistance, and reliable performance is chosen. The probe of this resistance is in direct contact with the refrigerant. The flowmeter on the test bench measures flow using a Yokogawa AXF series electromagnetic flowmeter, which is simple to use. It has a long service life, a quick response time, and good stability. Table 3 provides information about the test bench's measuring devices and range accuracy.

Table 3. The measuring instruments used in the experimental platform.

Name	Sign	Type	Precision	Range
temperature sensor	T1–T14	Pt100	± 0.1 °C	–10~60 °C
pressure transducer	P1, P2	PTX5072-TC-A1-CA-H0-PA: 0–4 Mpa G	0.2% FS	0~4 MPa
differential pressure transducer	$\Delta P1$	PTX5072-TC-A1-CA-H0-PA: 1 bar D	0.2% FS	0~1 bar
differential pressure transducer	$\Delta P2$	PTX5072-TC-A1-CA-H0-PA: 0.5 bar D	0.2% FS	0~0.5 bar
refrigerant flowmeter	GR1	RHM015T1P1PM0MOG1N	2.0%	0~0.6 kg/min
refrigerant flowmeter	GR2	RHM03T1P2PM0M0G1N	2.0%	0~5 kg/min
electromagnetic flowmeter	GW1, GW2	AXF015G-D1AL1S-AD41-01B/CH	5.0%	0~6.3 m ³ /h
electromagnetic flowmeter	GW3	LDY-15S-21CC-12-01-0-(3)-6-10-00	5.0%	0~6.3 m ³ /h

2.1.2. Experimental Section

According to Figure 4, the experimental section is a circular tube casing structure. The outer tube is made of aluminum, and the inner tube is made of copper. The inner tube has a diameter of 7 mm, and the outer tube has a diameter of 15.6 mm. The tube wall thickness is 0.21 mm. The length of the entire experimental section is 2 m. The straight tube in front of the experimental section has the same diameter as the development section. There is another experimental section before and after to lessen the heat exchange with the outside environment. The outer section of the tube is wrapped in insulation cotton and insulation foam, which is called outer pipe insulation. The inner and outer surfaces of the inner pipe are thoroughly mechanically polished and cleaned with ethanol to reduce the impact of surface roughness on the pipe walls. R22 flows in the inner tube of the experiment, while water flows in the outside tube. In order to analyze the variations in the heat transfer coefficient on the side surface of R22 and the pressure drop in the tube under each factor as well as the behavior of bubbles during boiling, the heating of water in the outer tube induces subcooling boiling of R22 in the inner tube.

**Figure 4.** Schematic diagram of experimental section.

2.2. Experimental Procedure

The experimental device is primarily made up of four circuits, including the experimental section's water circulation circuit, refrigerant circulation circuit, pre-cooling treatment circuit, and subcooling treatment circuit. Figure 2 illustrates the device's main components and structural layout. The pump in the circuit changes the required mass flow rate for the experiment while the refrigerant R22 is circulated in the circuit. Electric heaters and glycol cryogenic tanks circulate the water in the water circuit while regulating the temperature to the desired level. To create the necessary experimental section, the refrigerant pre-cooling treatment loop and the subcooling treatment loop are set to the requisite temperature. Table 4 displays the experimental working conditions.

Table 4. Experimental conditions.

Working Substance	Entry Temperature	Flow Rate	Pressure
ethylene glycol-water solution	288 K	0.272 kg/s	1 atm
R22	277.15 K	0.016 kg/s	6 atm

The experiment is conducted in accordance with the following procedure after each piece of equipment on the laboratory bench has been installed and inspected:

1. To introduce glycol aqueous solution into the circuit, turn on the low-temperature circulating pump and start the chiller;
2. Charge the refrigerant, turn on the refrigeration system, and compare the refrigerant's temperature at the experimental section's entrance to the corresponding refrigerant saturation temperature. Keep the inaccuracy within the margin, ideally between 0.2 °C and 0.3 °C. To reach the necessary subcooling temperature, the electric heater and valve in the circuit are adjusted to stabilize the fluid temperature at the experimental section's input;
3. By switching the refrigerant pump in the refrigerant circuit, the fluid's mass flow rate is raised to the required test level, and the pressure in the experimental portion is maintained by regulating the circuit valve;
4. Once the experimental unit is operating without any problems, turn on the data gathering equipment and let it run until the experiment is complete;
5. After the experiment is finished, first shut down the plate heat exchangers HE2 and HE3, then wait for the refrigerant to cool in the circuit before shutting down the chiller. Then, shut down the data acquisition instrument, disconnect the entire power supply, check the condition of the experiment bench once more to ensure safety, and clean the surrounding area.

If anomalies are discovered during the experiment, the experiment under the working condition should be stopped immediately, and the experiment under the working condition should be repeated once the abnormality has been resolved.

2.3. Experimental Data Calculation

When the experimental system functions properly over time, it can be seen that the values of the system tend to stabilize. At this point, the fluid characteristics can be taken to be constant, and the heat transfer coefficient can likewise be taken to be constant. The experimental part is properly insulated and can be thought as adiabatic because it is cleaned and polished with ethanol, which reduces the impact of dirt and surface roughness on heat resistance. The experimental section's heat transfer equation is:

$$Q = \frac{\Delta t_m}{\frac{1}{\pi d_o L h_o} + \frac{1}{\pi d_i L h_i} + \frac{1}{2\pi\lambda L} \ln \frac{d_o}{d_i}} \quad (1)$$

The heat exchange required in the experimental section is provided by the water flow in the counter-current arrangement of the outer tube, and the heat exchange Q is:

$$Q = q_m C_p \Delta T \quad (2)$$

The logarithmic mean temperature difference between the inner tube refrigerant temperature and the outer tube heating water temperature in the experimental section is:

$$\Delta t_m = \frac{\Delta t_{max} - \Delta t_{min}}{\ln \frac{\Delta t_{max}}{\Delta t_{min}}} \quad (3)$$

where Δt_{max} and Δt_{min} are, respectively, the greater and smaller of the temperature differentials between the heating water's inlet and outlet and the refrigerant's intake and outlet of the experimental portion. The "Heat Exchanger Design Manual" [28] has the heat trans-

fer coefficient for heating water flowing on the outside of the tube with an intake $Re > 1000$ for turbulent flow, and it is computed as follows:

$$\frac{h_o \cdot d_e}{\lambda_l} = 0.023 Re^{0.8} Pr^{0.4} \left(\frac{D_o}{D_i} \right)^{0.45} \quad (4)$$

From Equations (1)–(4), the boiling heat transfer coefficient in the tube h_i can be calculated, and the required physical properties for data calculation are obtained by checking the software REFPROP 8.0.

2.4. The Uncertainty Analysis of the Experiment

Due to the accuracy level of the measuring instrument, there will also be systematic errors during the experiment. In order to improve the credibility of the experimental data, the Moffat method is used to analyze the uncertainty of important data.

Moffat's uncertainty calculation method is:

It is assumed that a series of parameters affecting U are:

$$U = U(X_1, X_2, X_3, \dots, X_n) \quad (5)$$

Then the combined uncertainty of U is:

$$\delta U = \left\{ \sum_{i=1}^n \left(\frac{\partial U}{\partial X_i} \delta X_i \right)^2 \right\}^{0.5} \quad (6)$$

After calculation, the uncertainty of the experimental data is shown in Table 5.

Table 5. Experimental uncertainty.

Name	Sign	Precision
temperature sensor	T1–T14	±0.1 °C
pressure transducer	P1, P2	±0.2%
differential pressure transducer	ΔP1, ΔP2	±0.2%
refrigerant flowmeter	GR1, GR2	±2.0%
electromagnetic flowmeter	GW1, GW2, GW3	±5.0%

2.5. Experimental Result

When the required refrigerant temperature is set to 4 °C, the inlet temperature of the experimental section reaches and stabilizes at 3.87 °C at approximately 100 s. Although the set temperature is not reached, this is related to the system error and other related factors. However, the difference from the set target is very small. Therefore, the experimental platform can better control the realization of the refrigerant inlet subcooling state. In addition, it can be seen that the refrigerant outlet temperature fluctuates around 5.53 °C, indicating that the flow state of the fluid in the tube is supercooled flow.

The analysis of Figure 5d shows that the inlet pressure of the experimental platform reaches 6 atm. Therefore, the experimental platform can better complete the pressure value corresponding to the subcooled flow of the refrigerant at the inlet.

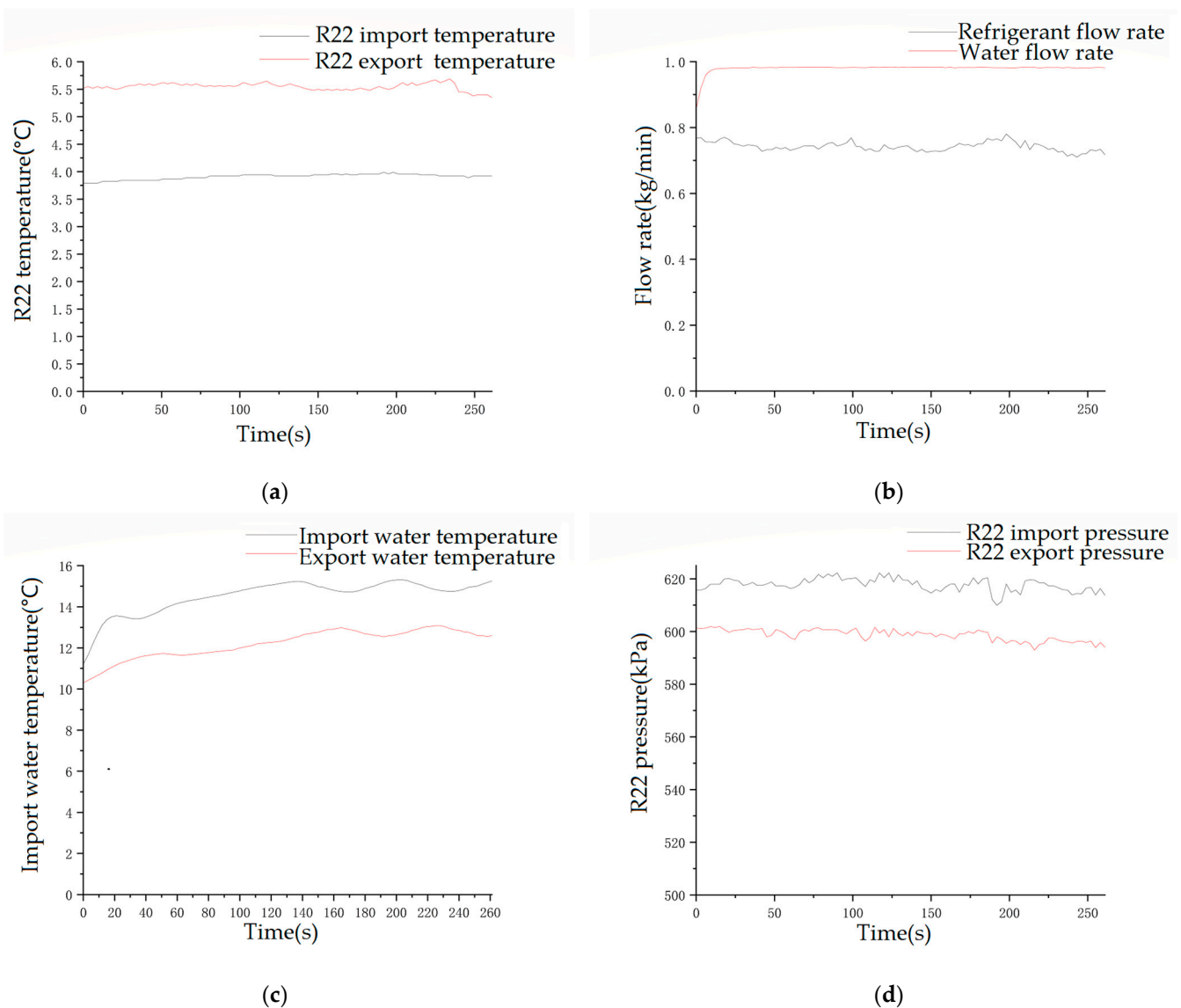


Figure 5. The subcooled flow boiling experiments of R22 in a horizontal casing tube are depicted in Figure 5, along with the changes in each data point over time. (a) Refrigerant temperature versus time curve; (b) curves of the flow rate of each working fluid changing with time; (c) heated water temperature with time curve; (d) refrigerant pressure versus time curve. Subcooling boiling occurs when an unsaturated liquid flows into a tube and is heated by the wall of the tube; the liquid near the wall then reaches a temperature above saturation and begins to bubble, while the main body of the liquid has not yet reached saturation. The saturated nucleation boiling zone is reached if the fluid is heated further until the mainstream reaches the saturation temperature. Given its excellent insulation and disregarding the thermal resistance of the ground, the experimental segment of the pipe can be thought to have reached thermal equilibrium. The experimental section's rear sight glass S4 is used to observe the gas–liquid two-phase flow while the refrigerant inlet temperature is 4 °C for subcooling. The subcooling boiling occurs during the experiment, and some of the heat transfer of water is converted into the latent heat of refrigerant vaporization, according to the experimental data. The heat transfer of heated water and the heat gain of R22 are calculated using the Equation (9), and the heat transfer of water is greater than the heat gain of R22.

The analysis of Figure 5c shows that the inlet temperature of water in the experimental section reaches 15.25 °C, which achieves the experimental results. After the water passes through the experimental pipe section, the outlet temperature shows a downward trend and finally stabilizes at 12.59 °C. The evaporation temperature of the water in the exper-

imental tube section is 100 °C. Therefore, it can be determined that the water side of the experimental section is single-phase flow. According to Equation (1), the amount of heat exchange provided by water for refrigerant measurement can be calculated. The specific heat capacity of water is 3.56 kJ/(kg·K) and its density is 1054.31 kg/m³. According to Figure 5b, the water flow rate of the experimental pipe section is 0.98 m³/h. The heat provided by water per unit time is calculated to be 2.74 kJ/s. Assuming that the refrigerant R22 is a single-phase flow, the energy absorbed by the refrigerant is calculated to be 0.0116 kJ/s according to Equation (2). The specific heat capacity of R22 is 0.675 kJ/(kg·K). According to Figure 5b, the flow rate of R22 in the experimental pipe section is 0.72 kg/min. According to the principle of energy conservation, it can be judged that R22 is not a single-phase flow in the tube. Therefore, it can be explained that the refrigerant R22 undergoes a phase change in the tube, and the phase change process is accompanied by latent heat. The latent heat of R22 is 200.11 kJ/kg, which can completely absorb the energy provided by the hot water measurement. Through the analysis of the temperature, pressure, and energy of the subcooled flow of R22 in a single tube, it can be obtained that the single tube experimental platform can complete the subcooled flow experiment and that the phase change occurs in the tube. However, there is a lack of visualization, so further exploration is needed.

3. Numerical Simulation Research Methods

Based on the experimental data collected during the studies, the presence of flow boiling was confirmed, providing solid data support for the ensuing simulation work. This chapter develops the numerical model of R22 subcooled boiling in a casing tube and sets up the simulation method.

3.1. Numerical Model Selection

3.1.1. Multiphase Flow Model

ANSYS is a software company founded on the fundamentals of CFD (Computational Fluid Dynamics) which contains a wealth of physical models. By combining the study object with the chosen model and completing the convergence of the solution, the simulation can be finished. In addition to the aforementioned information, the VOF method is chosen as the interface tracking method in ANSYS to create the VOF model.

The VOF method introduces a discontinuous scalar function F in the whole flow field. Its value is a real number between 0 and 1. When $F = 0$, it means that there is only one flow phase in this grid. When $F = 1$, it means that this grid contains only another flow phase. If the value of F is between 0–1, it means that the grid contains two different flow phases at the same time. And the size of the value expresses the proportion of the two flow phases in this grid. The fluid interface is located in the grid. The schematic of the VOF method is shown in Figure 6.

The function F is called the phase volume fraction. The VOF method uses the phase volume fraction function F to determine the phase interface and track the change in the fluid, rather than tracking the movement of the particles and the marker points on the phase interface. It presents a new basic idea of phase interface construction and opens up a new field of numerical simulation of moving phase interfaces. Compared with other methods, the VOF method occupies less computer storage space and has low requirements on computer hardware, especially when dealing with three-dimensional problems. The calculation of the VOF method is simple and the phase interface is clear, which can show the structure and change of complex phase interfaces. The VOF method is superior to other phase interface tracking methods in dealing with the fusion and fragmentation of complex phase interfaces and three-dimensional phase interfaces. Therefore, it can be applied to the simulation of various practical projects.

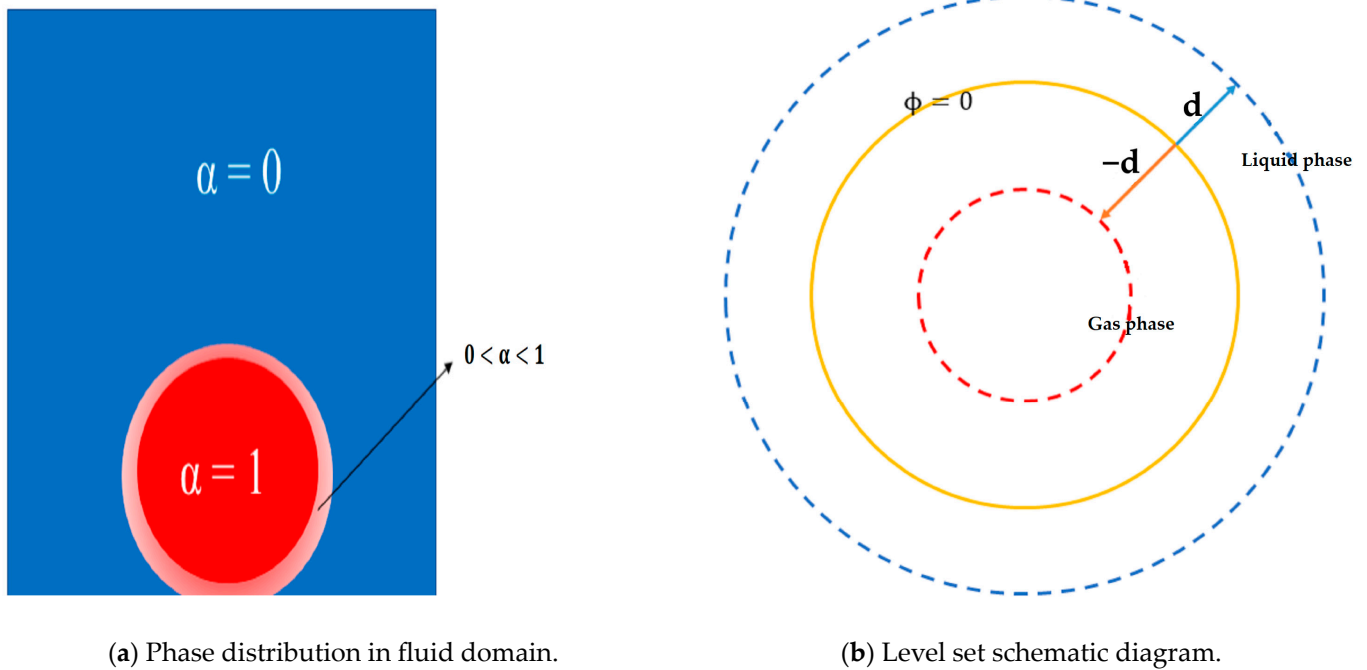


Figure 6. Schematic of the VOF method.

The value is stated as follows in the VOF model by keeping track of the volume fraction in each cell grid:

$$\alpha = \begin{cases} 0 & \text{Liquid phase} \\ 0 < \alpha < 1 & \text{Interface} \\ 1 & \text{Gas phase} \end{cases} \quad (7)$$

When $\alpha = 0$, it indicates that this cell grid contains only the liquid phase. When $\alpha = 1$, it indicates that the value in this cell grid contains the gas phase. When the value of α is between 0 and 1, it means that the cell grid contains both gas and liquid phases. In other words, there is a gas–liquid interface.

The continuity equation for the gas phase is:

$$\frac{\partial \alpha_v}{\partial t} + \nabla \cdot (\vec{u} \alpha_v) = \frac{S_{M-lv}}{\rho_v} \quad (8)$$

The continuity equation for the liquid phase is:

$$\frac{\partial \alpha_l}{\partial t} + \nabla \cdot (\vec{u} \alpha_l) = \frac{S_{M-ol}}{\rho_l} \quad (9)$$

$$\alpha_l + \alpha_v = 1 \quad (10)$$

The velocity field obtained by solving a single momentum equation in the full domain is shared between the liquid phase and the gas phase. The liquid and gas phases share a set of momentum and energy equations.

The momentum equation is:

$$\frac{\partial \rho \vec{u}}{\partial t} + \nabla \cdot (\rho \vec{u} \vec{u}) = -\nabla p + \nabla \cdot [\mu_{eff} (\nabla \vec{u} + \nabla \vec{u}^T)] + \rho \vec{g} + \vec{F}_{vol} \quad (11)$$

The energy equation is:

$$\frac{\partial \rho c_p T}{\partial t} + \nabla \cdot (\vec{u} (\rho c_p T + p)) = \nabla \cdot (\lambda_{eff} \nabla T) + S_E \quad (12)$$

In Equations (11) and (12), surface curvature κ_l , mixture density ρ , mixture viscosity μ , mixture specific heat capacity c_p , and mixture conductivity λ are as follows:

$$\kappa_l = \nabla \cdot \frac{\nabla \alpha}{|\nabla \alpha|} \quad (13)$$

$$\rho = \alpha_l \rho_l + \alpha_v \rho_v \quad (14)$$

$$\mu = \alpha_l \mu_l + \alpha_v \mu_v \quad (15)$$

$$c_p = \alpha_l c_{pl} + \alpha_v c_{pv} \quad (16)$$

$$\lambda = \alpha_l \lambda_l + \alpha_v \lambda_v \quad (17)$$

The control equation with the level set method:

$$\frac{\partial \phi}{\partial t} + \nabla \cdot (\vec{\mu} \phi) = 0 \quad (18)$$

where ϕ is symbolic distance function and the zero iso-surface of ϕ is used to track the vapor–liquid interface.

The definition of symbolic distance function ϕ :

$$\phi(x, t) = \begin{cases} d(x, \{x \in \Omega | \phi(x, t) = 0\}) & x \in R \\ 0 & x = \{x \in \Omega | \phi(x, t) = 0\} \\ -d(x, \{x \in \Omega | \phi(x, t) = 0\}) & x \in R \end{cases} \quad (19)$$

The effective dynamic viscosity μ_{eff} is:

$$\mu_{eff} = \mu + \rho \nu_t \quad (20)$$

The effective thermal conductivity λ_{eff} is:

$$\lambda_{eff} = \lambda + \rho c_p \frac{\nu_t}{Pr_t} \quad (21)$$

Among the various forces affecting the behavior of bubbles, surface tension plays a dominant role, including bubble nucleation, growth, and rupture. In this paper, a continuous surface tension (CSF) model is used in the simulation work to convert the surface tension into a bulk force, that is, the effect of surface tension is added into the momentum equation [29]. \vec{F}_{vol} in Equation (11) can be defined as:

$$\vec{F}_{vol} = \sigma \frac{\rho \kappa_l \nabla \cdot \alpha_l}{0.5(\rho_l + \rho_v)} \quad (22)$$

3.1.2. Turbulence Model

The casing model utilized in this experiment has an inner tube diameter of only 7 mm, making it a narrow channel with a smaller Reynolds number that is more noticeable near the wall. The turbulence model should be used to account for the low Reynolds number since the subcooling boiling process generates a lot of bubbles that can impact the flow. It is required to select a turbulence model in order to anticipate the boiling because of the shear impact brought on by near-wall turbulence during subcooled boiling. The SST k- ω model takes into account the effect of shear stress and combines it with the k- ω model for the low Reynolds number region near the wall, which greatly improves the accuracy and stability of turbulence simulations [30].

Therefore, the SST k - ω model is used in the simulation, where the transport equations for k and ω are:

$$\frac{\partial \rho k}{\partial t} + \nabla \cdot (\rho k \vec{u}) = \nabla \cdot \left[\left(\nu + \frac{\nu_t}{\sigma_k} \right) \nabla \cdot k \right] + G_k - Y_k \quad (23)$$

$$\frac{\partial \rho \omega}{\partial t} + \nabla \cdot (\rho \omega \vec{u}) = \nabla \cdot \left[\left(\nu + \frac{\nu_t}{\sigma_\omega} \right) \nabla \cdot \omega \right] + G_\omega - Y_\omega + D_\omega \quad (24)$$

$$\nu_t = \rho \frac{k^2}{\omega} \frac{1}{\max\left[\frac{1}{a^*}, \frac{SF_2}{a_1 \omega}\right]} \quad (25)$$

Because the k - ω model is still for fully developed turbulence, and for the boundary layer near the wall, a combination of wall functions is needed to accurately describe the flow in the tube. Introduced to denote the distance from the outermost fluid unit to the adjacent wall, the bubbles depart from the boundary layer belonging to the buffer region, which is the region where viscosity and Reynolds stress are evident, according to the characteristics of flow boiling [31].

$4 < y^+ < 20$ ensures that the near-wall region belongs to the buffer region. y^+ is defined as:

$$y^+ = \frac{y u_\tau}{\nu} \quad (26)$$

3.1.3. Phase Transition Model

It is frequently important to include a source term in the numerical simulation in order to more accurately replicate the phase transition process in the gas–liquid phase. The Lee model, which is driven by the temperature difference between the interface temperature and the saturation temperature, is selected as the phase transition model in this article. The phase transition occurs when the fluid temperature is equal to the saturation temperature. The source term's precise form is as follows:

The liquid phase source term is:

$$S_{M-lv} = -\eta \alpha_l \rho_l \frac{T - T_{sat}}{T_{sat}} \quad (if \ T > \ T_{sat}) \quad (27)$$

The gas phase source term is:

$$S_{M-vl} = \eta \alpha_v \rho_v \frac{T_{sat} - T}{T_{sat}} \quad (if \ T < \ T_{sat}) \quad (28)$$

The energy source term is:

$$S_E = h S_M \quad (29)$$

The simulation uses the Lee model as the phase transition model and is embedded into the UDF.

3.2. Physical Modeling

In order to compare and analyze the effects of external tube heating water flow rate, refrigerant inlet flow rate, and subcooling degree on the heat transfer coefficient and to investigate the bubble behavior of R22 in subcooled flow boiling, numerical simulations of refrigerant flow subcooled boiling heat transfer inside the casing are carried out in this section.

This research chooses to reduce the actual problem to a physical model, focusing on the physical problem in a two-dimensional geometric model due to the limitations of the experimental simulation equipment. In this study, we use AutoCAD 2019 software to model the outer tube at 15.6 mm, the inner tube at 7 mm, and tube length at 2000 mm in a 2D geometric model, which is shown in Figure 7. Nine points of "0, 0, 0", "0, 7, 0", "0, 15.6, 0", "0, -7, 0", "0, -15.6, 0", "2000, 7, 0", "2000, 15.6, 0", "2000, -7, 0", "2000, -15.6, 0" were established. The experiment involves the flow of R22 in the inner tube and water in the

outer tube in a counter-flow configuration. This causes subcooling and boiling of R22 in the inner tube due to heat transfer with the water in the outer tube, allowing the study of changes in the heat transfer coefficient and bubble behavior of the R22 side surface under each factor.

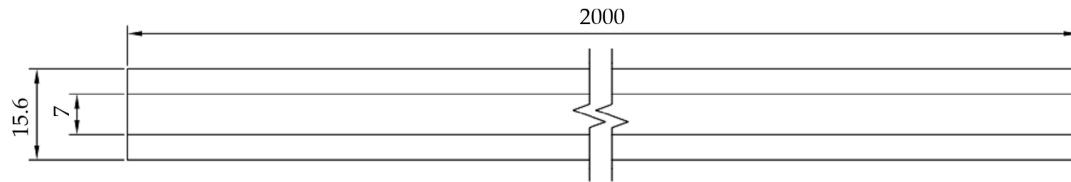


Figure 7. Physical model of pipe section.

To produce the mesh file, one must import the constructed 2D surface model into ICEM 19.0, create blocks, associate the geometric model's points, lines, and surfaces, configure node parameters, generate the mesh, and encrypt the mesh on the inner pipe wall. When dividing the lines, the number of points set on the long side line is 130, the number of points set on the short side line is 45, and the inner tube wall is encrypted to 0.05. The created mesh file is imported into FLUENT for the numerical simulation calculation, convergence, and iterative results checking, and finally the simulation data and bubble clouds are obtained in the post-processing to finish the simulation. The finished mesh is schematically separated using ICEM, as seen in Figure 8. Due to the straightforward principles of the computing domain, the paper employs a quadrilateral grid. The quadrilateral grid has good precision, is straightforward to converge and is suitable for basic and regular geometric models. The outer tube outlet is directly connected to the atmosphere, the inner tube continuously maintains the pressure inside the tube, and the outlet boundary type is set to pressure outlet. The liquid phase and gas phase velocities can be calculated through the flow and geometric models. Some of the boundary conditions are shown in Table 6.

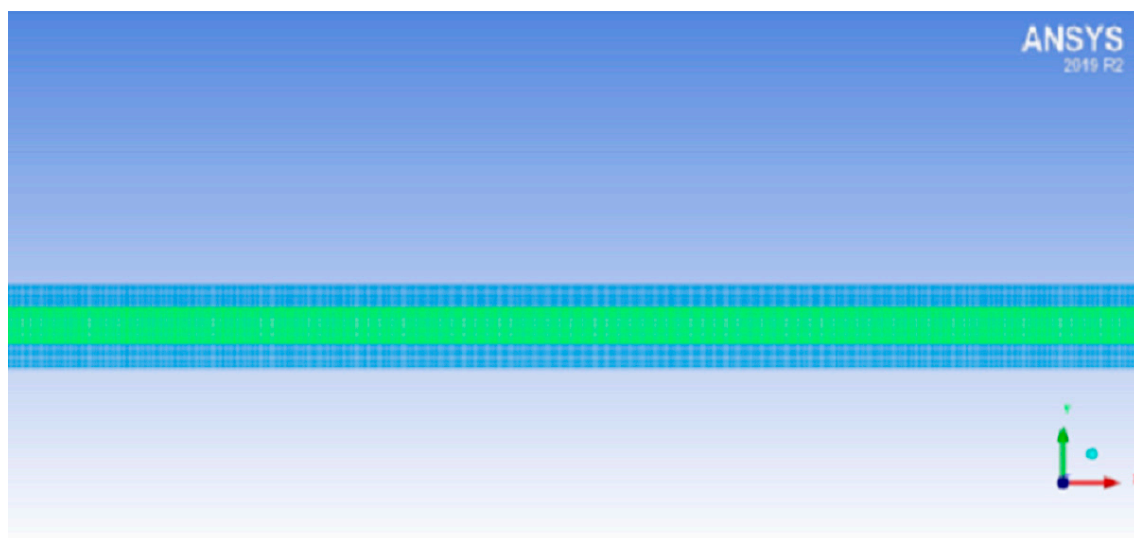


Figure 8. Schematic diagram of grid model.

Table 6. Structural dimensions and part boundary condition.

Component	Dimensions (mm)	Component	Boundary Condition
Inlet diameter	7	Inlet	Speed inlet
Outer diameter	15.6	Outlet	Pressure outlet
Length	2000	Inner wall	Heat
		Outer wall	Wall
		Gap	Fluid

On the basis of the computational region developed in this paper, a quadrilateral grid is chosen. Quadrilateral meshes have the advantages of rapid convergence and excellent computational accuracy, making them suitable for straightforward and regular geometric models. The velocities of the liquid and gas phases can be determined using the flow rate and geometric model, allowing the inlet boundary condition to be set to velocity inlet. The inner tube maintains a constant pressure inside the tube, establishing the outlet boundary condition as a pressure outlet. The outlet of the outer tube is connected to the atmosphere. In order to restrict fluid movement and heat transfer, the outer wall boundary type of the casing is chosen as a wall boundary, and the inner wall boundary type is chosen as a heat boundary in order to conduct heat transfer on this wall.

Certain assumptions are made regarding the fluids simulated in this article in order to acquire more accurate simulation results while focusing on the nature of heat transfer in the tube and speeding up the simulation. The fluid in the pipe is assumed to be a continuous medium, meaning that it continuously changes a variety of microscopic physical properties. The fluid in the pipe is first considered to be a non-spin, non-pressurized fluid. If bubble generation can be smoothly discharged, then the fluid in the pipe does not reflux.

3.3. Calculation Scheme

In order to run the simulations, FLUENT 19.0 was used. A pressure-based, transient, two-dimensional solver was employed. The PISO method was used for the calculations and PRESTO was used to interpolate the pressure. In order to collect interface fluxes and ensure accurate tracking of the most precise interface, the geo-reconstruction method was adopted for interface reconstruction. The sub-relaxation factors for the remaining parameters are left at their default values. The sub-relaxation factor was set to 0.3 for pressure, 0.3 for momentum and energy, and 0.3 for volume force. In Table 7, other parameters are displayed.

Table 7. Calculation method related settings.

Entry	Setting
discrete method of energy and momentum equations	Second-order upwind
turbulent kinetic energy	First-order upwind
specific dissipation rate	First-order upwind
level-set function	Second-order upwind
time step	1×10^{-5}
gradient discrete format	Green–Gauss node-based method

The simulation used 48 threads of computer processing power and 5 TB of memory. The data file was saved every 10 s for time steps, every 1×10^{-5} s for time steps, and every 250 s for the number of time steps in the final calculation settings. After testing, one simulation case used 210 GB of memory and took 24 h to complete.

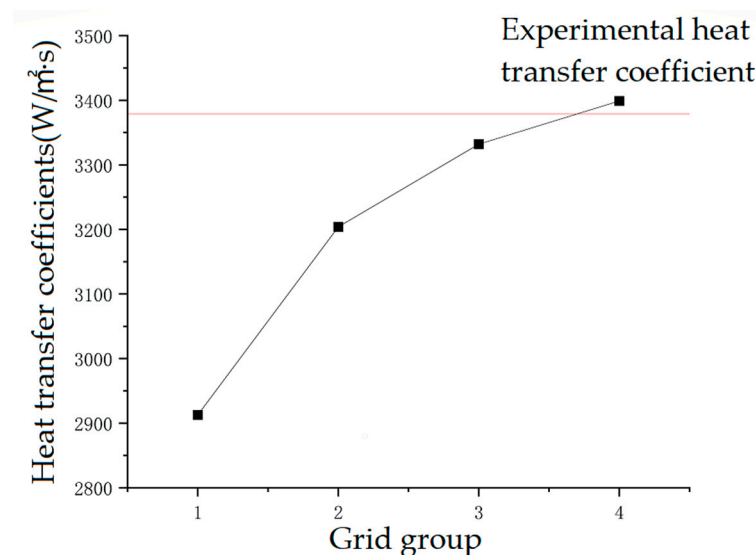
3.4. Grid Independence Test and Numerical Model Validation

In this study, the mesh file was created and the boundary conditions were defined using ICEM. A mesh independence check is necessary because the size and quality of the mesh influence the outcome and convergence of the numerical simulation. In general, the faster the calculation, the smaller the mesh, but the less accurate the results and the more prone you are to divergence and errors. This is especially true in the case of phase changes, when having insufficient meshes might affect the tracking of bubble behavior. Conversely, as the number of meshes increases, the computation becomes slower, but the results get more precise and convergent. As a result, it is critical to choose the right number of meshes for the real model while accurately accounting for computing time. The number of structured meshes developed for this simulation, which were divided into four groups, is displayed in Table 8. In the region of the inner tube's refrigerant sidewall surface that was to be analyzed, all four groups of grids were encrypted.

Table 8. Number of grids.

Grid Numbering	1	2	3	4
Grid number	85,800	99,000	132,000	165,000

The above four groups of grids were numerically simulated for R22 subcooled boiling in this study using the same working conditions and the simulation calculation results were compared with the actual experimental data, as shown in Figure 9. It can be seen that the simulation results match real values more closely the more meshes there are. The results are nearly identical to the experimental values when the simulations are run using grids No. 3 and 4. This shows that the calculated results are independent of the number of grids and satisfy the requirements for grid independence. The difference between the simulated data of grid No. 3 and grid No. 4 is only 1.8%. On the other hand, the chosen computational model has a high degree of accuracy and satisfies the needs of the simulation work, as evidenced by the consistency of the computational results and experimental data. Therefore, grid No. 3 is selected for the numerical simulation due to its processing resources and power limitations.

**Figure 9.** Grid independence and numerical model verification.

It is important to note that in the simulation, which satisfied the requirements of the SST $k-\omega$ model, y^+ is in the range of four to sixteen (i.e., it belongs to the buffer region). As a result of the buffer region's considerable viscous and Reynolds stresses in the SST $k-\omega$ model, the bubble growth environment was more accurately approximated.

4. Results and Discussion

The research work focuses on the effects of changes in refrigerant mass flow rate, heating water mass flow rate, refrigerant inlet temperature, and dryness on the R22 boiling heat transfer coefficient by examining the outcomes of numerical simulations of refrigerant R22 boiling in subcooled flow in a horizontal casing. In order to increase the efficiency of heat transmission and better show the heat transfer process, the bubble behavior of subcooled boiling in R22 tubes is also examined.

4.1. Boiling Heat Exchange Analysis

4.1.1. Inner Tube Refrigerant Mass Flow Rate

By altering the refrigerant mass flow rate, a numerical simulation of R22 boiling in subcooled flow in a horizontal casing is carried out to investigate the impact of refrigerant flow rate variation on the boiling heat transfer coefficient in a horizontal tube. All other

parameters remain the same. Figure 10 illustrates the relationship between the boiling heat transfer coefficient on the R22 side and tube length for various refrigerant flow rates. The boiling heat transfer coefficient of the R22 side wall of the inner tube increases as the flow rate in the tube increases, and the two exhibit a positive correlation. A liquid layer will form on the tube wall as the refrigerant flows and boils, preventing heat exchange and increasing thermal resistance. The inner tube wall's liquid film is strengthened, and the flow of refrigerant is accelerated, which improves the heat exchange between the refrigerant and the tube wall. The boiling heat transfer coefficient increases by 10.7% when the refrigerant mass flow rate rises from 0.016 kg/s to 0.018 kg/s, as shown in Figure 10. When the refrigerant mass flow rate was increased from 0.018 kg/s to 0.020 kg/s, the boiling heat transfer coefficient improved only by 2.2%, showing that the same mass flow rate increment did not strengthen the boiling heat transfer coefficient as much as in the low mass flow rate area. This could be because of the narrow channel's influence. A high mass flow rate will increase the disturbance of the refrigerant mass flow, which intensifies the convective heat transfer between the mass and the wall. But this hinders the formation of the bubble nucleation point and consequently affects the occurrence of nucleation boiling, resulting in a decrease in heat transfer performance.

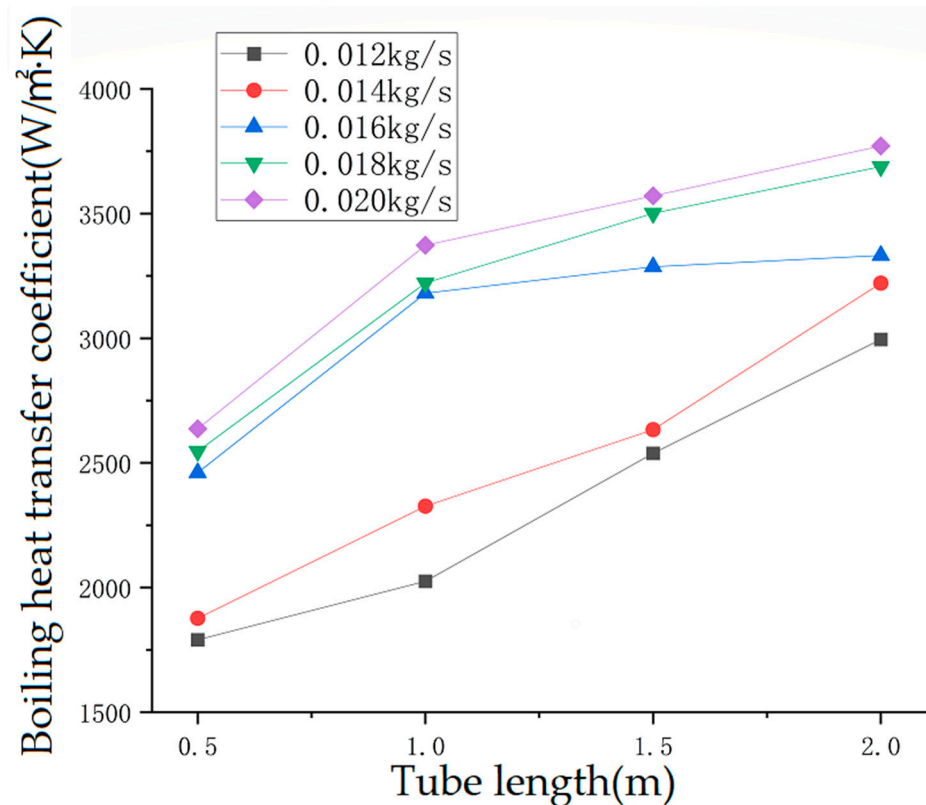


Figure 10. The change of boiling heat transfer coefficient with refrigerant mass flow rate.

4.1.2. Outer Tube Heating Water Mass Flow Rate

The mass flow rate of water heated by the outer tube is changed in a numerical simulation of R22 boiling in a horizontal casing with subcooling flow in order to study the impact of this change on the boiling heat transfer coefficient in the horizontal tube. All other conditions remain the same. The trend of the boiling heat transfer coefficient on the R22 side with tube length for various external tube heating water flow rates is depicted in Figure 8. The boiling heat transfer coefficient increases along with the flow of water heated by the outer tube, and the two are positively connected. A water–glycol solution is poured

into the outer tube, acting as an anti-freeze and giving the inner tube the necessary heat flow density. The Dittus–Boelter formula states:

$$Nu_f = 0.023Re_f^{0.8}Pr_f^{0.4} \quad (30)$$

The Equation (30) shows that the flow rate enhances the heat transfer efficiency of the outer tube by increasing the density of heat flow. The intensification of nucleation boiling and the development of additional gasification cores are all made possible by the rise in heat flow density, which also enhances the superheat of the inner tube wall surface. The boiling heat transfer coefficient rises with the mass flow rate of water heated by the outer tube, or the heat flow density, as shown in Figure 11. The boiling heat exchange coefficient increases quickly when the flow of hot water leaving the tube reaches 0.340 kg/s. Therefore, it can be said that one of the key elements influencing R22's subcooled boiling is the heat flow density. When the flow of heated water outside the tube is between 0.136 kg/s and 0.272 kg/s, the boiling heat transfer coefficient gradually increases. The slower boiling rate and excessive lag between supercooled boiling and saturated boiling are caused by the reduced heat flow density.

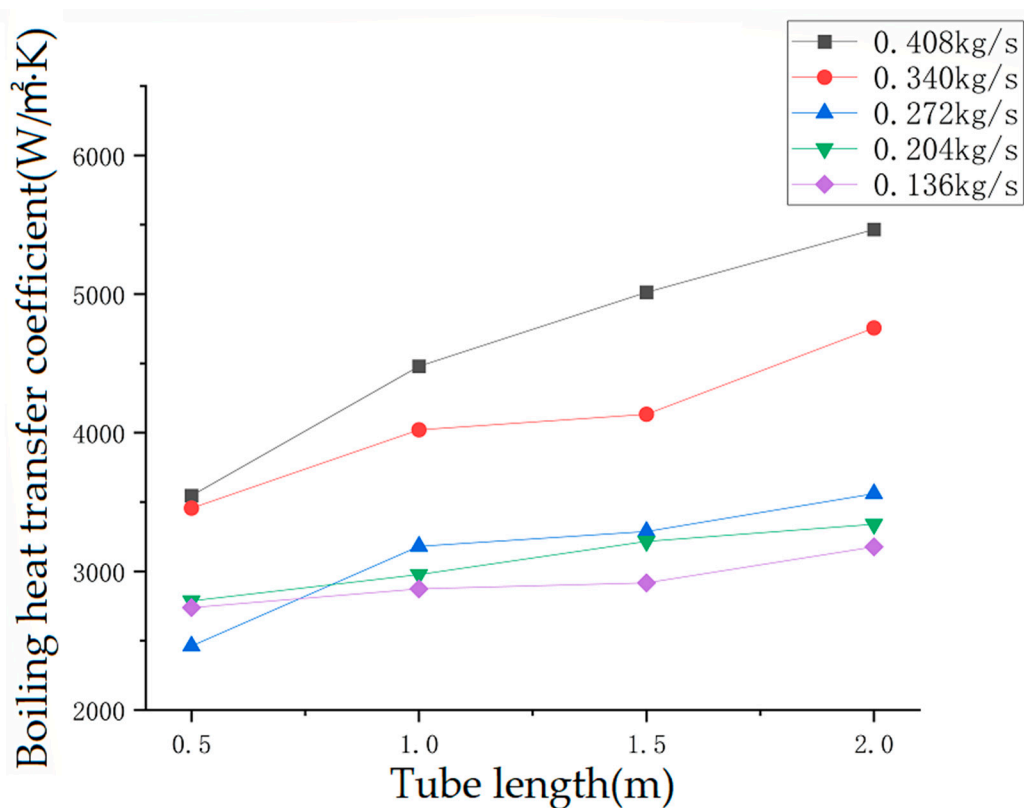


Figure 11. The variation of boiling heat transfer coefficient with the mass flow rate of heated water.

4.1.3. Inner Tube Refrigerant Inlet Temperature

The numerical simulation of R22 boiling in subcooled flow in a horizontal casing is carried out by changing the inner tube refrigerant inlet temperature. Other conditions remain unchanged in order to study the effect of inner tube refrigerant inlet temperature variation on the boiling heat transfer coefficient in a horizontal tube. The trend of the boiling heat transfer coefficient of the R22 side with tube length for various inner tube refrigerant inlet temperatures is depicted in Figure 12.

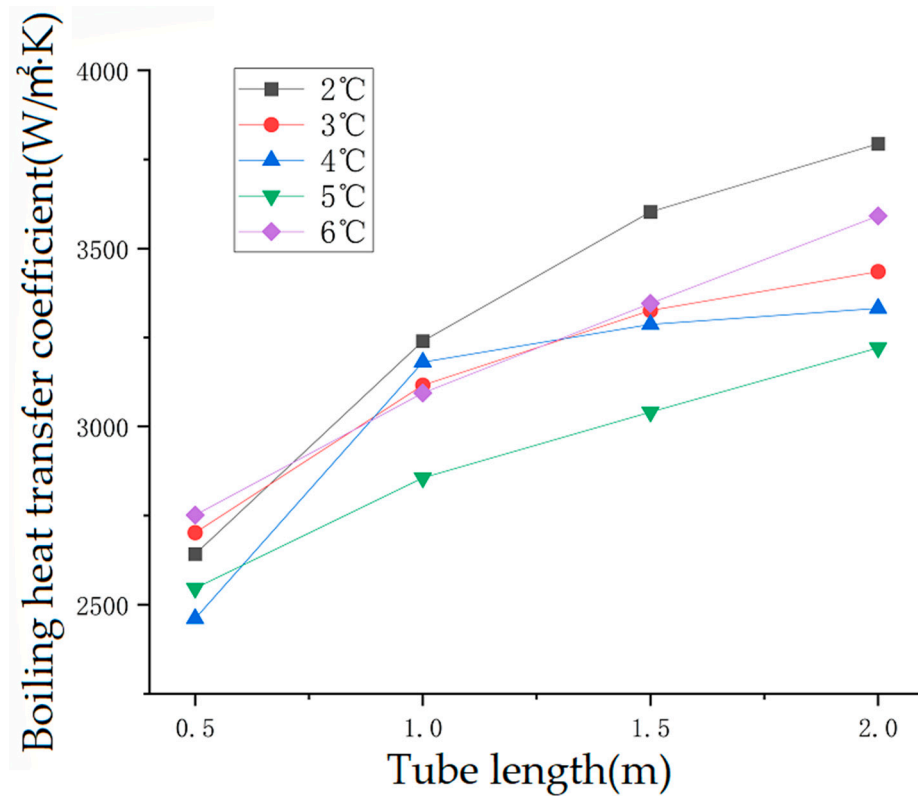


Figure 12. The change of boiling heat transfer coefficient with the inlet temperature of refrigerant.

Low inlet temperature fluid achieves substantial subcooling, which in turn generates a significant temperature difference with the wall surface to facilitate heat transfer, increasing the boiling heat transfer coefficient of the refrigerant. Convective heat transfer predominates near the input section at this temperature because bubble formation is inhibited and reaching the ONB point is difficult due to the significant subcooling. As a result, the initial heat transfer coefficient is high and increases slowly. Boiling is necessary for high subcooling, which increases heat transmission to some extent while simultaneously requiring a greater latent heat of vaporization.

Because the refrigerant at the inner tube's inlet easily reaches the ONB point at a tube pressure of 6 atm and the saturation evaporation temperature of R22 is approximately 7 °C, the boiling heat transfer coefficient of the refrigerant still rises as the inlet temperature rises. The refrigerant's gas content rises as the inlet temperature rises, and the flushing action on the liquid coating that prevents heat exchange is strengthened. Additionally, when the inlet temperature rises, the refrigerant's physical characteristics also change. Its density and viscosity decrease, while the disruption of the fluid flow increases, strengthening convective heat transfer.

What needs to be explained is that y^+ is in the range of four to sixteen (i.e., it belongs to the buffer region) in the simulation, which met the conditions of the SST $k-\omega$ model. In the SST $k-\omega$ model, the viscous and Reynold stresses were significant in the buffer region, so it follows that the bubble growth environment was more realistically simulated.

4.2. Bubble Behavior Analysis

The numerical simulation was performed using the experimental conditions for the two-dimensional horizontal casing model (Figure 4): 288 K water temperature at the inlet of the outer pipe, 0.272 kg/s water flow rate, and 1 atm water pressure; 277.15 K water temperature at the inlet of the inner pipe R22, 0.012 kg/s refrigerant flow rate, and 6 atm refrigerant pressure. The experimental data is loaded into the Tecplot 360 EX 2021 R2

software when the simulation is finished in order to evaluate the bubble images and track the behavior of the bubbles.

4.2.1. Sliding of Bubbles

- Sliding of the detached bubble

In Figure 13, the red rectangle frame depicts the nucleation, slide, departure, and collapse of bubbles during subcooled boiling. It is noted that this process is the dominant one in boiling. The bubble begins to form at 8.35 ms, slides at 8.35 ms, achieves its peak volume at 8.65 ms, separates from the tube wall at 9.25 ms, and eventually bursts at 9.4 ms. The force imbalance of the bubble is the main cause of bubble sliding. The bubble is impacted by buoyancy force, surface tension, pressure, etc. When the force acting in the horizontal direction is out of proportion, the bubble begins to slide, and when the force acting in the vertical direction is out of balance, the bubble breaks free from the wall. The near-wall superheated layer, the microfluid layer at the bottom of the bubble evaporating, and the supercooled mainstream condensing all have the biggest effects on the bubbles during this process. The heating surface, as depicted in Figure 14, offers superheat for the sloshing of bubbles. The boiling heat transfer coefficient of the wall surface is significantly increased as a result of this procedure.

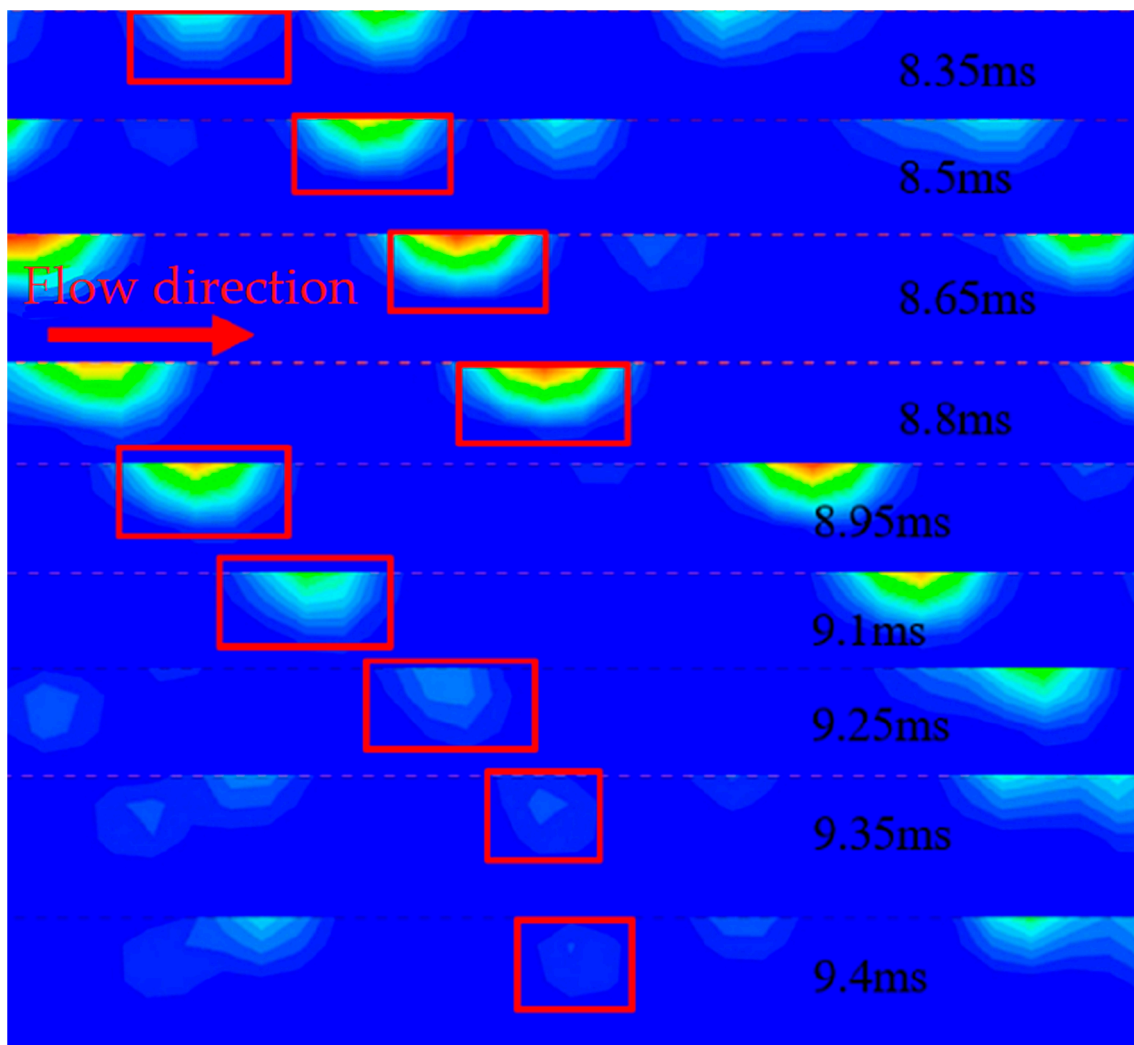


Figure 13. Bubble sliding.

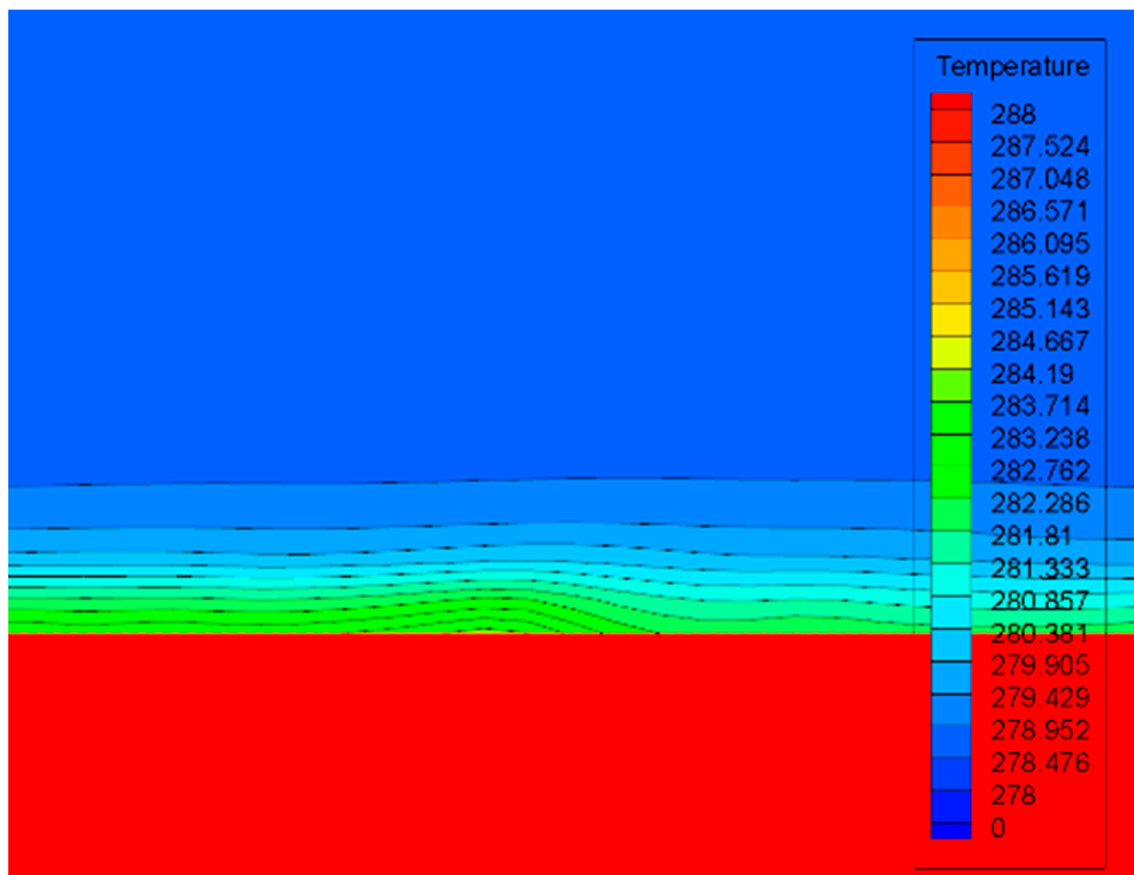


Figure 14. The temperature gradient at the heating surface.

- Sliding without detaching the bubble.

Unseparated bubbles are another phenomenon that occurs in supercooled flow boiling. Figure 15 illustrates the slide process of an uncoupled bubble, which directly collapses rather than leaving the heated wall. Such detached sliding bubbles frequently form at the pipe entrance when supercooled boiling is just starting to take place and the buoyancy force supplied is insufficient to offset the force acting on the bubble in the vertical direction because of the low superheat of the wall. The bubble's axial velocity steadily lowers during the sliding, as seen in the picture, and this deceleration tendency may create a favorable environment for the expansion of the sliding bubble.

It has been agreed that bubble sliding and departure are driven by multiple forces, surface tension, shear lift force, quasi-steady drag force, and buoyancy. Surface tension is the resistance during bubble sliding. The drag force deforms the bubble during the top movement of the bubble, while the buoyancy makes the bubble have a tendency to leave the wall. Furthermore, other forces are opposite to surface tension. The surface tension hinders the growth of the bubble. The shear force affects the radial bubble motion. Moreover, the surface tension, shear lift force, and quasi-steady drag force fluctuate during sliding, which might be caused by the fluctuation of bubble velocity [32].

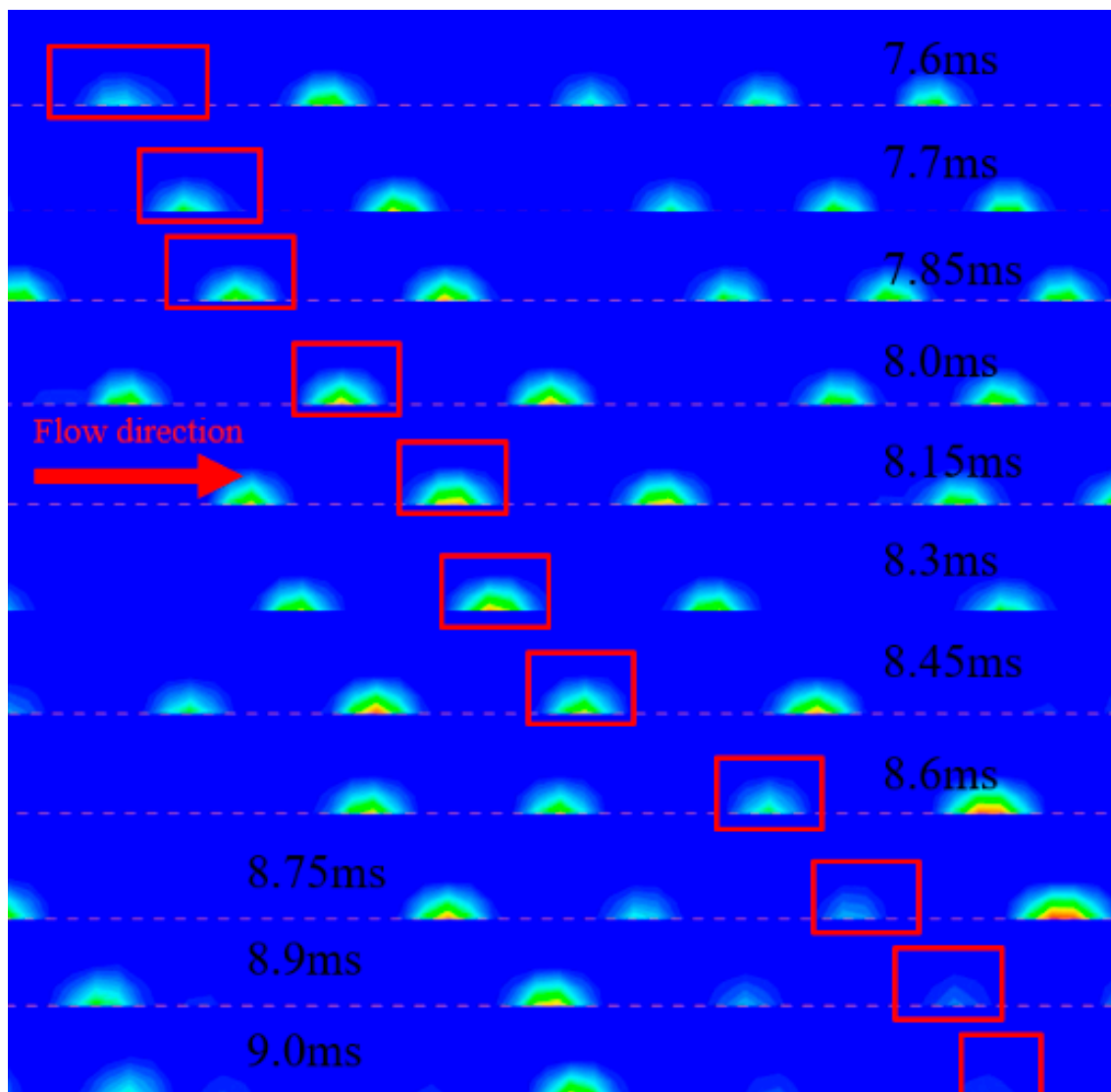


Figure 15. The growth process of bubbles.

4.2.2. Bubble Aggregation

According to Figure 16, the two bubbles collide and begin to interact at 9.4 ms, fuse at 9.9 ms, and finish aggregating at 10.2 ms. According to conventional wisdom, when the flow is stable in the horizontal tube with uniform heat transfer, the main factors affecting the aggregation of subcooled flow boiling bubbles are bubble collision and relative motion caused by turbulent flow, and the aggregation of bubble rupture makes the flow phase more complex in favor of turbulent heat transfer.

4.2.3. Bubble Bounce

According to Figure 17, bubbles left the wall at 8.8 ms, but they did not immediately collapse. Instead, they approached the mainstream and became condensed, which reduced the size of the bubble. At 9.55 ms, the bubble was condensed and started to move toward the wall. At 9.7 ms, it was re-attached to the wall and continued to slide and grow. This process is dominated by the bubbles' surface tension, which causes the bubbles to reattach to the heated walls.

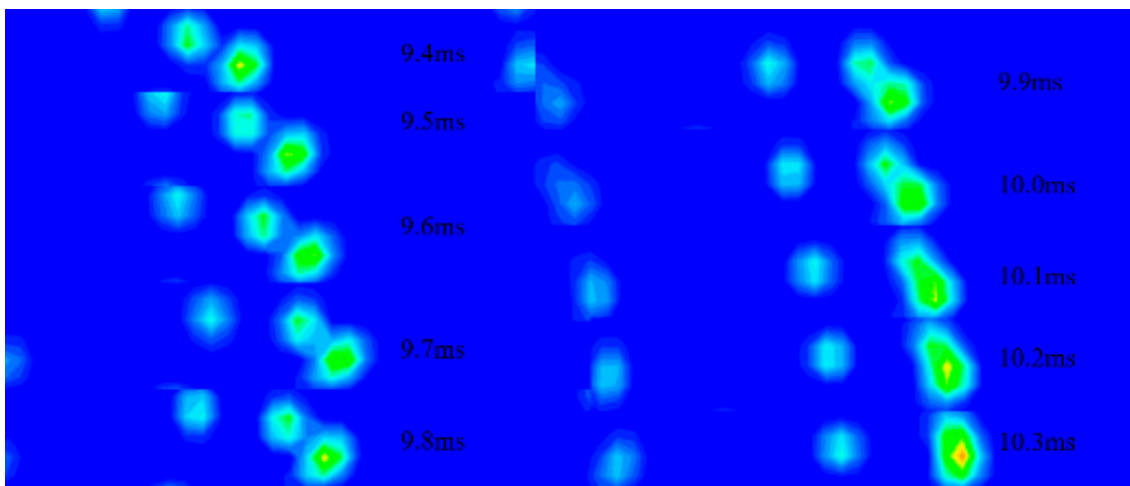


Figure 16. Bubble aggregation.

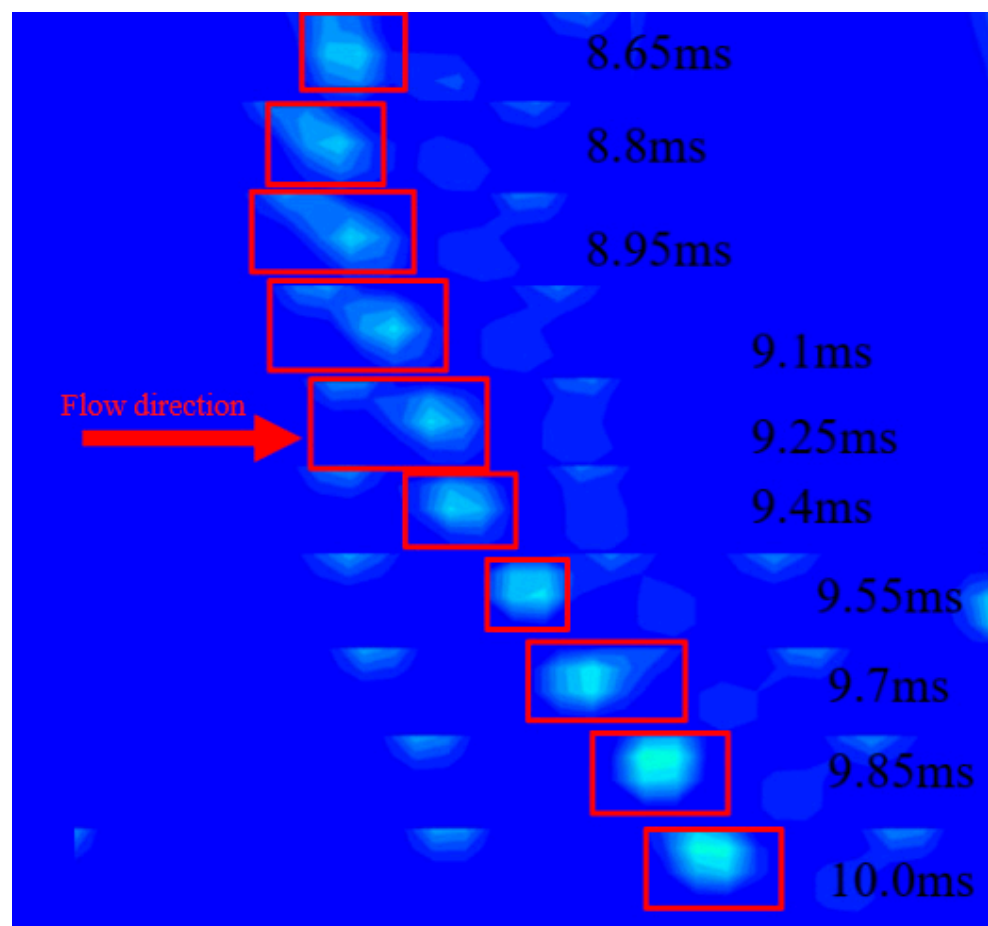


Figure 17. Bubble bounce.

5. Conclusions

A complex multiphase flow with applications in many different industries and the subcooling flow boiling of a small channel refrigerant offers considerable research potential. This work investigates experimentally and numerically the subcooled boiling of R22 in a horizontal case. The effects of the flow rates of the refrigerant, the heating water, and the subcooling of the refrigerant on the wall's boiling heat transfer coefficient were

investigated and evaluated. Bubble images were also produced, and bubble behavior was simulated and examined. The following are the key findings:

- In the horizontal light pipe, the boiling heat transfer coefficient of R22 increases with an increase in refrigerant mass flow rate. However, with the same increase in flow rate, the effect of heat transfer in the high refrigerant mass flow rate region, between 0.018 kg/s and 0.020 kg/s, is less significant than that in the low refrigerant mass flow rate region, between 0.016 kg/s and 0.018 kg/s. Consequently, a suitable increase in the refrigerant mass flow rate can aid in improving boiling heat exchange.
- The boiling heat exchange coefficient increases with the flow of water heated by the outer tube, and the increase is evident in the subcooling flow boiling of R22 in the casing. The main goal of increasing the flow of water heated by the outer tube is to increase the density of heat flow to the test tube section, which raises the inner tube wall surface's superheat and causes more vaporization core formation and faster ONB point arrival. Since increasing the heat flow density has a considerable impact on improving heat exchange, it can be said that the heat flow density is one of the major parameters influencing the heat exchange of R22 subcooling boils.
- The boiling heat transfer coefficient of R22 in the horizontal light pipe varies more intricately with the refrigerant inlet temperature. When the input temperature is too low, the subcooling degree is 5 °C. This causes a bigger temperature differential, which increases convective heat transfer and increases the boiling heat transfer coefficient of R22. When the inlet temperature is higher than the subcooling degree of 1 °C, the boiling heat exchange coefficient of R22 increases because the inlet temperature has been close to the saturation temperature at this pressure. The refrigerant is easily able to reach the ONB point, the boiling heat exchange is intense, and the physical properties of the refrigerant will also be changed due to the high temperature, so the flow disturbance is enhanced and the heat exchange is strengthened.
- Beyond the fundamental bubble behavior, the subcooled boiling bubble behavior in the flow of R22 in the casing is complex. This work concentrates on three types of subcooled boiling bubble behavior: The sliding of the dominant bubble, which completes nucleation, sliding, departure, and collapse, is primarily influenced by the superheated layer in the near-wall region; evaporation of the micro-liquid layer at the bottom of the bubble; and condensation of the supercooled main stream. The primary causes of bubble aggregation are collisions between bubbles and relative motion caused by turbulent flow. The bouncing effect of bubbles is caused by surface tension.

6. Limitations of the Study and Prospects for the Future

- R22 is a refrigerant that needs to be replaced under the “Montreal Protocol”, with a production and use cut-off date of 2030 in China. Due to the limitations of the experimental facilities, R22 refrigerant is selected for research in this paper. Subsequent research on new refrigerants can be carried out using this experimental method and the established numerical model.
- In this paper, a two-dimensional model is used to simulate the subcooled flow boiling in the casing tubes. Because the actual experimental process is carried out in a three-dimensional tube, the use of a two-dimensional model will cause a certain degree of distortion. The simulation equipment used in this paper has limited computing power and cannot perform large-scale, high-precision three-dimensional simulations, so further research is needed.
- The experimental section of the test bench is a closed, invisible tube. In the subsequent experiments, the visible tube should be used with a high-speed camera to capture the actual bubble behavior.

Author Contributions: Conceptualization, X.H. and F.W.; methodology, X.H.; software, X.H.; validation, X.H., B.W. and F.W.; formal analysis, X.H.; investigation, X.H.; resources, X.H. and J.X.; data curation, F.W.; writing—original draft preparation, F.W.; writing—review and editing, X.H. and

J.W.; supervision, J.X.; project administration, J.X.; funding acquisition, J.X. All authors have read and agreed to the published version of the manuscript.

Funding: This research was funded by the National Key R&D Program of China, grant number 2019YFD0901604; Science and Technology Innovation Action Plan of the Shanghai Science and Technology Commission, grant number 19DZ1207503; and the Public Service Platform Project of the Shanghai Science and Technology Commission, grant number 20DZ2292200.

Data Availability Statement: The research data of this paper can be obtained from the corresponding author “Wang Jinfeng” or “Xie Jing” through reasonable request.

Acknowledgments: The support of Shanghai Ocean University, China, is gratefully acknowledged.

Conflicts of Interest: The authors declare no conflict of interest.

Abbreviations

Nomenclature

C_p	constant pressure specific heat [kJ/(kg · K)]
D	casing pipe diameter (m)
D	tube diameter (m)
G	Gravity (m/s^2)
H	boiling heat transfer coefficient [$W/(m^2 \cdot K)$]
K	turbulent kinetic energy ($m^2 \cdot s^{-2}$)
M	mass source [$kg/(m^3 \cdot s)$]
P	pressure (N/m^2)
P_r	prandtl number
Q	transfer quantity (W)
q_m	mass flow rate (kg/s)
Re	Reynolds number
T	mixture temperature (K)
ΔT	temperature difference (K)
Δt_m	the logarithmic mean temperature difference ($^{\circ}C$)
T	Time (s)
\vec{u}	Velocity (m/s)
\vec{u}^T	Transpose part of strain rate tensor
u_{τ}	shear velocity (m/s)
y^+	turbulence length-scale
y	boundary layer length (m)
α	volume of fraction

Greek symbols

κ	surface curvature (1/m)
λ	Heat conductivity [$W/(m^2 \cdot K)$]
v	Vapor
ρ	Density (kg/m^3)
σ	coefficient of surface tension (N/m)
ω	turbulent vortex frequency

Nomenclature

eff	Effective
i	inner tube
l	Fluid
$M - vl$	liquid phase to gas phase
o	outer tube
p	Pressure
sat	Saturation
v	Vapor
$vl - M$	gas phase to liquid phase
vof	Volume

References

1. Dedov, A.V. A review of modern methods for enhancing nucleate boiling heat transfer. *Therm. Eng.* **2019**, *66*, 881–915.
2. Tao, W.Q. *Heat Transfer*, 5th ed.; Higher Education Press: Beijing, China, 2019.
3. Lim, J.H.; Park, M. Forced convective and sub-cooled flow boiling heat transfer in a hypervapotron heat sink under one-side heating condition. *Int. J. Heat Mass Transf.* **2022**, *186*, 122–523.
4. Kong, L.J. *Study of Subcooled Boiling Heat Transfer Characteristics and Bubble Behaviors in Helically-Coiled Tubes*; Shandong University: Jinan, China, 2016.
5. Zhou, Z.R.; Chen, Y.Z.; Hao, L.M. *Research on Subcooled Flow Boiling under High Heat Flux and Its Application*; Nanjing University of Aeronautics and Astronautics: Nanjing, China, 2018.
6. Zhang, H.X.; Chen, Y.Z.; Hao, L.M. Evaluation of the typical CHF correlations, models and the 95 CHF Look-up table of sub-cooled water flow boiling under low pressure. *Nucl. Sci. Eng.* **2002**, *2*, 111–116+129. [[CrossRef](#)]
7. Wang, X.J.; Chen, B.D.; Huang, Y.P. Simulation of vertical upward sub-cooled boiling flow in a pipe. *CIESC J.* **2007**, *6*, 1353–1358.
8. Lucchini, A.; Carraretto, I.M.; Phan, T.N.; Pittoni, P.G.; Colombo, L.P. Comparison between R134a and R1234ze(E) during flow boiling in microfin tubes. *Fluids* **2021**, *6*, 417. [[CrossRef](#)]
9. Shin, J.Y.; Kim, M.S.; RO, S.T. Experimental study on forced convective boiling heat transfer of pure refrigerants and refrigerant mixtures in a horizontal tube. *Int. J. Refrig.* **1997**, *20*, 267–275. [[CrossRef](#)]
10. Gungor, K.E.; Winterton, R.H.S. A general correlation for flow boiling in tubes and annuli. *Int. J. Heat Mass Transf.* **1986**, *29*, 351–358.
11. Gungor, K.E.; Winterton, R.H.S. Simplified general correlation for saturated flow boiling and comparisons of correlations with data. *Chem. Eng. Res. Des.* **1987**, *65*, 148–156.
12. Saisorn, S.; On, J.K.; Wongwises, S. Flow pattern and heat transfer characteristics of R-134a refrigerant during flow boiling in a horizontal circular mini-channel. *Int. J. Heat Mass Transf.* **2010**, *53*, 4023–4038.
13. Wang, S.M.; Jian, G.P.; Xiao, J.; Wang, J.R.; Wen, J. Multi-Objective Optimization on the Structural Parameters of Spiral Wound Heat Exchanger. *J. Xi'an Jiaotong Univ.* **2017**, *51*, 9–15.
14. In, S.; Jeong, S. Flow boiling heat transfer characteristics of R123 and R134a in a micro-channel. *Int. J. Multiph. Flow* **2009**, *35*, 987–1000. [[CrossRef](#)]
15. Welch, J.E.; Harlow, F.H.; Shannon, J.P.; Daly, B.J. *The MAC Method—A Computing Technique for Solving Viscous, Incompressible, Transient Fluid-Flow Problems Involving Free Surfaces*; Los Alamos Neutron Science Center: New Mexico, NM, USA, 1996.
16. Uchihashi, Y.; Yaegashi, Y.; Matsuo, M. Improvement of a simple coupled VOF with LS (S-CLSVOF) method. *J. Chem. Eng. Jpn.* **2023**, *56*, 2197456. [[CrossRef](#)]
17. Amina; Norio, T. Numerical investigation of 3D flow properties around finite emergent vegetation by using the two-phase Volume of Fluid (VOF) modeling technique. *Fluids* **2022**, *7*, 175.
18. Mulbah, C.; Kang, C.; Mao, N.; Zhang, W.; Shaikh, A.R.; Teng, S. A review of VOF methods for simulating bubble dynamics. *Prog. Nucl. Energy* **2022**, *154*, 104478.
19. Tao, S.; Shi, G.; Xiao, Y.; Huang, Z.; Wen, H. Effect of operating parameters on the coalescence and breakup of bubbles in a multiphase pump based on a CFD-PBM coupled model. *J. Mar. Sci. Eng.* **2022**, *10*, 1693. [[CrossRef](#)]
20. Dai, D.Z. *Numerical Simulation of Gas-Liquid Two-Phase Flow Based on VOF Method*; Nanjing University of Aeronautics and Astronautics: Nanjing, China, 2014.
21. Khan, Z.A.; Ahmad, N.; Sattar, M.; Haq, M.A.; Khan, I.; Ganie, A.H. Cell alternation algorithm for simulating bubble growth in boiling flows through volume of fluid (VOF) method in fluent. *Alex. Eng. J.* **2022**, *61*, 13051–13066. [[CrossRef](#)]
22. Liu, Z.W.; Bo, H.L. Two-dimensional Euler grid approximation method for multi-droplet motions. *Int. Commun. Heat Mass Transf.* **2023**, *145*, 106825.
23. Li, S.; Lu, C.; Zhang, C.; Li, Z.; Zhao, J.; Chen, J.; Wei, N. Modeling and investigation of fluid flow affecting thermal boundary conductance at the solid-fluid interface. *Int. J. Heat Mass Transf.* **2023**, *213*, 124333.
24. Yang, G.Q.; Bing, D.; Fan, L.S. Bubble formation and dynamics in gas-liquid-solid-fluidization-A review. *Chem. Eng. Sci.* **2007**, *62*, 2–27.
25. Li, Y.; Zhang, J.P.; Fan, L.S. Discrete-phase simulation of single bubble rise behavior at elevated pressures in a bubble column. *Chem. Eng. Sci.* **2000**, *55*, 4597–4609. [[CrossRef](#)]
26. Li, Y.; Yang, G.Q.; Zhang, J.P.; Fan, L.S. Numerical studies of bubble formation dynamics in gas-liquid-solid fluidization at high pressures. *Powder Technol.* **2001**, *116*, 246–260.
27. Dijkhuizen, W.; Van den Hengel, E.I.; Deen, N.G.; van Sint Annaland, M.; Kuipers, J.A. Numerical investigation of closures for interface forces acting on single air-bubbles in water using Volume of fluid and front tracking models. *Chem. Eng. Sci.* **2005**, *60*, 6169–6175. [[CrossRef](#)]
28. Wei, L.H.Y. *Heat Exchanger Design Manual*; Petroleum Industry Press: Beijing, China, 1982.
29. Oratis, A.T.; Bush, J.W.; Stone, H.A.; Bird, J.C. A new wrinkle on liquid sheets: Turning the mechanism of viscous bubble collapse upside down. *Science* **2020**, *369*, 685–688. [[CrossRef](#)] [[PubMed](#)]
30. Baltussen, M.W.; Kuipers, N.G.D. A critical comparison of surface tension models for the volume of fluid method. *Chem. Eng. Sci.* **2014**, *10*, 10965–10974. [[CrossRef](#)]

31. Owoeye, E.J. *Bubble Transport in Subcooled Flow Boiling*; University of Florida: Gainesville, FL, USA, 2015.
32. Yu, B.; Wang, J.; Xie, J.; Wang, B.; Wang, F.; Deng, M. Bubble Sliding Characteristics and Dynamics of R134a during Subcooled Boiling Flow in a Narrow Gap. *Mathematics* **2023**, *11*, 2197.

Disclaimer/Publisher's Note: The statements, opinions and data contained in all publications are solely those of the individual author(s) and contributor(s) and not of MDPI and/or the editor(s). MDPI and/or the editor(s) disclaim responsibility for any injury to people or property resulting from any ideas, methods, instructions or products referred to in the content.